

# Modeling short crack propagation under variable structural and thermal loadings

Alexander Bosch<sup>1,2</sup>  | Michael Vormwald<sup>3</sup> 

<sup>1</sup>Department of Materials Technology, MTU Aero Engines AG, Munich, Germany

<sup>2</sup>Technische Universität Darmstadt

<sup>3</sup>Materials Mechanics Group, Technische Universität Darmstadt, Darmstadt, Germany

## Correspondence

Alexander Bosch, Department of Materials Technology, MTU Aero Engines AG, Dachauer Str. 665, 80995 Munich, Germany.  
Email: alexander.bosch@mtu.de

## Funding information

AiF

## Abstract

In the present work, a new concept for the prediction of fatigue life under variable structural and thermal loads is presented based on the modeling of short crack propagation by the effective cyclic  $J$ -integral. Stresses in the range below the initial endurance limit up to plastic deformations can be considered. The development and validation of the concept is based on the large database of constant and variable amplitude loading tests for the austenitic stainless steel X6CrNiNb18-10 (1.4550, AISI 347). Taking into account the influence of notches and welding process, tests were performed for specimens with different stress concentration factors and even with specimens of nonhomogeneous microstructure due to welding or its physical simulation (Gleeble). The input for the developed model is based on local stress–strain hysteresis in the order of their occurrence. This is the basis for considering load sequence effects; the new  $J$ -based model considers several types of them. The model as well as the identification of the parameters will be presented in detail. Validation to experimental results is also shown against the background of common fatigue concepts. Basic aspects of the model are discussed.

## KEYWORDS

crack propagation,  $J$ -integral, short crack growth, thermomechanical fatigue

## 1 | INTRODUCTION

Due to the increasing use of renewable energies, power plants are operated more and more flexibly. The originally stationary operation, which was only interrupted by shutdowns and commissioning for regular inspections, has become a demand-oriented operation. By this operation mode, the additional load is expressed in a high number of smaller load changes. The load cycles themselves are mainly induced by temperature changes. The guidelines for the design and assessment of such components (e.g., KTA3201.2<sup>1</sup> or ASME Code Section VIII<sup>2</sup>) focus on the evaluation of the thermomechanical start–

stop cycle. The resulting elastic–plastic strain amplitudes clearly assign the stress situation to the low cycle fatigue (LCF) regime. Those elastic–plastic strain amplitudes were estimated from a linear-elastic calculation to which a plastification factor ( $K_e$  factor) is applied as a function of load height. Furthermore, the calculations are based on a reference temperature, so the material and damage behavior is taken into account independently of temperature. Further, important factors influencing the fatigue life of the components such as the mean stresses and the sequence effects in case of variable amplitude loading or also the influence of the component's size are covered rather generally by providing the Wöhler line for the

This is an open access article under the terms of the Creative Commons Attribution-NonCommercial License, which permits use, distribution and reproduction in any medium, provided the original work is properly cited and is not used for commercial purposes.

© 2021 The Authors. Fatigue & Fracture of Engineering Materials & Structures published by John Wiley & Sons Ltd.

strain amplitudes with corresponding factors. Against the background of this initial situation, manufacturers and operators of power plants (with any kind of power generation) have an increased need for a more realistic assessment of the fatigue life under service loads. The request goes so far that the calculation method is online capable and shows the corresponding danger potential in the context of a power plant monitoring. As a result of the many simplifications, an adequate evaluation of welded and unwelded components and parts under variable structural-mechanical and thermal loads with consideration of plastic deformations is not possible at the present time.

The actors involved are aware that, especially in the presence of possibly large plastic deformations, load sequence effects occur which lead to much shorter lifetimes than those calculated with the classical Palmgren–Miner<sup>3,4</sup> rule. This linear damage accumulation rule assumes under variable amplitude loading that the frequency  $n_i$  of cycles at load level  $i$  causes a numerical contribution to the damage sum normalizing  $n_i$  by the number of cycles to failure  $N_i$  under constant amplitude loading. The damage sum contributions are supposed to add up linearly:

$$D = \sum_{i=1}^k \frac{n_i}{N_i}. \quad (1)$$

As for constant amplitude loading, the failure damage sum is assumed to be  $D = 1.0$ . The greatest shortcoming of this rule is that the sequence of the occurring stress and strain cycles cannot be considered, although this has a very large influence on the lifetime. To be able to display sequence effects at all, the material element and with it, the mechanically loaded component must be able to store information about the load history. In the field of mechanics, there are only two possible memory storages for load histories: plastic deformation and material separation.<sup>5</sup> Nevertheless, the task of sequence recording in the damage accumulation calculation has not yet been fully solved. The present special issue with contributions to the fourth Conference on Variable Amplitude Loading is an eloquent testimony of ongoing research activities on this topic. It is beyond the intention of this paper to give a comprehensive overview of the damage accumulation problem. The still current overviews of Fatemi and Yang<sup>6</sup> and Skorupa<sup>7,8</sup> give a first insight into the matter.

The first step in determining the influence of plastic deformation history on service life is to simulate it for the possible locations of engineering cracking. The local strain approach is available for this purpose. Dowling<sup>9</sup> has composed its elements. The German Research Association for Mechanical Engineers has published a comprehensive set of rules for standardized application (FKM guideline nonlinear).<sup>10,11</sup> The approach presented here follows this

guideline in its basic version; extensions and further developments are introduced where appropriate.

The guideline<sup>11</sup> specifies damage parameter life curves for assessing fatigue lives to technical crack initiation. One of the two parameters,  $P_{RAJ}$ , is derived from the cyclic  $J$ -integral. The origin of this parameter goes back to Vormwald and Seeger<sup>12</sup>, still under the name  $P_J$ . The procedure assumes the existence of a short crack, whose growth rate is linked to the cyclic  $J$ -integral by a power law. The sequence effects were captured realistically by including a history variable for the crack opening strains in the simulation of the elastic–plastic stress–strain path. An adjustment of mean stress sensitivities and size effects was done in later publications.<sup>13,14</sup> In the guideline,<sup>11</sup> the fatigue life calculation is transferred from an integration of the crack growth rate to a damage accumulation calculation of the Palmgren–Miner type. In the present paper, this is discarded.

The concepts developed, which take into account both the mean stresses and the load history as well as the temperature dependence individually on the load side, are based on the  $P_J$  concept. Improvements are made by substituting of the crack propagation law and performing a crack propagation calculation instead of a damage accumulation. Further improvements are made for the modeling of the transition of the threshold for small cracks to long cracks and the consideration of transient crack closure. The concept variants differ in the crack propagation law and the consideration of transient crack closure in style of Anthes,<sup>15</sup> but all of them can be applied even under variable temperatures. All concept variants share the relatively easy identification of the required parameters, which are to be determined mainly using results of constant amplitude loading and static tension tests. The advantages of the improvements and the fracture mechanics-based approaches are shown in contrast to the results of conventional approaches. The developed concept is discussed in connection with additional load sequence effects. The present paper is an extended version of the paper published in the proceedings of the fourth Conference on Variable Amplitude Loading.<sup>16</sup>

## 2 | EXPERIMENTAL CAMPAIGN

### 2.1 | Material


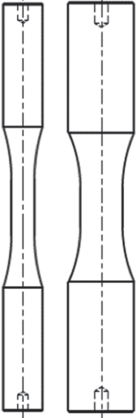



In a joint research project, the experimental investigations<sup>17,18</sup> focused on the metastable austenitic stainless steel X6CrNiNb18-10. It is a commonly used steel for components of pressurized components of light water reactors in Germany. In this project, a variety of models were developed for assessing variable amplitude fatigue under isothermal as well as thermomechanical loading

conditions. After the end of the project, some models were further developed. The paper at hand presents the current state of model development and the results of the lifetime calculations achievable with it. A presentation of all details, the reproduction of which would go beyond the scope of this paper, can also be found in the monograph by Bosch.<sup>19</sup>

Many austenitic steels show a plasticity-induced phase transformation when mechanically loaded at room temperature.<sup>20,21</sup> The material investigated here does not make an exception. However, the maximum operating temperature of the components of interest is about  $\sim 370^\circ\text{C}$ . While a phase transformation from austenite to martensite is observed at room temperature, this phenomenon does not occur under higher temperatures. Especially, when temperature variations between 50 and  $370^\circ\text{C}$  were applied as done in the present investigation, the formation of martensite could not be observed. For most of the isothermal experiments performed, a temperature of  $180^\circ\text{C}$  was chosen, which is the mean temperature in operation.

## 2.2 | Specimens and testing

A variety of different specimens are tested. From a scientific point of view, it is desirable to separate the sequence effects from the size effects. For this reason, a large number of experiments were carried out on almost unnotched material specimens, which are shown in Figure 1 as hourglass, smooth, weld, or Gleeble specimens. The notation IWM indicates that the experiments have been performed in the laboratory of the research partner Fraunhofer Institute of Materials Mechanics, Freiburg. IFSW states that the test were done in the laboratory of the authors. At IWM, all described tests were performed on a Walter and Bai electromechanical testing machine with inductive heating; at IFSW, all described tests were performed on a servo hydraulic testing machine with convective heating. Further information concerning the test experimental setup is given in the final report of the abovementioned research project.<sup>17</sup>

Type	Hourglass (HG) specimen (IFSW)	Smooth specimen (IWM)	Notch specimen (IFSW)	Weld specimen (IWM)	Gleeble specimen (IWM)
Shape					
Material	base material	base material	base material	base material/ weld material	heat affected zone (HAZ)
Additional characteristics			geometrical notch $r = 1\text{mm}$	metallurgical and geometrical notch $r \sim 0,01\text{mm}$	simulated characteristics of HAZ
	$d = 5\text{mm}$	$d = 7\text{mm}$ $/(d = 8\text{mm})$	$d = 5,5\text{mm}$	$d_1 = 12\text{mm}$ $d_2 = 4\text{mm}$	$d = 8\text{mm}$
	$K_t = 1,02$ $K_f \sim 1,00$	$K_t = 1,00$ $K_f = 1,00$	$K_t = 1,57$ $K_f = 1,26$	$K_t = 3,00$ $K_f = 1,93$	$K_t = 1,00$ $K_f = 1,00$

**FIGURE 1** Overview of specimen types by geometry, material, special characteristics, diameter in nominal section (for weld specimen outer diameter  $d_1$  and diameter of inner drill  $d_2$ ), stress concentration, and effective stress concentration factor used for calculations

The specimens labelled ‘Gleeble’ have undergone temperature–time sequences as they were measured in the heat-affected zone (HAZ) of the weld specimens during the weld process. Further information of physical simulations and especially the applied welding simulation can be gained by the supplier<sup>22</sup> of Gleeble systems. The tests on notched and welded specimens are intended to show that the findings on variable amplitude life calculation obtained on unnotched specimens can also be used to evaluate the structural durability of components.

Notched and welded specimens are characterized by a stress concentration factor of  $K_t = 1.57$  and  $K_t = 3.0$ , respectively, both associated with the net section nominal stress and determined by FE analyses. Mainly due to the statistic size effect, their notch fatigue factors are reduced to  $K_f = 1.26$  and  $K_f = 1.93$ . The constant amplitude life curves were calculated by applying the local strain approach in connection with the material's life curve, the notch approximation procedure by Neuber,<sup>23</sup> and an adjusted fixing of the notch fatigue factors. The notch fatigue factors were used instead of the stress concentration factors to obtain comparable fatigue lives numerically under constant amplitude loading of notched and welded specimens based on material parameters for HG and smooth specimens. Those fatigue factors, derived from constant amplitude loading test, were also used for calculations under variable amplitude loading. Considering the statistical size effect following FKM guideline<sup>24</sup> would have provided nearly the same numbers.<sup>19</sup>

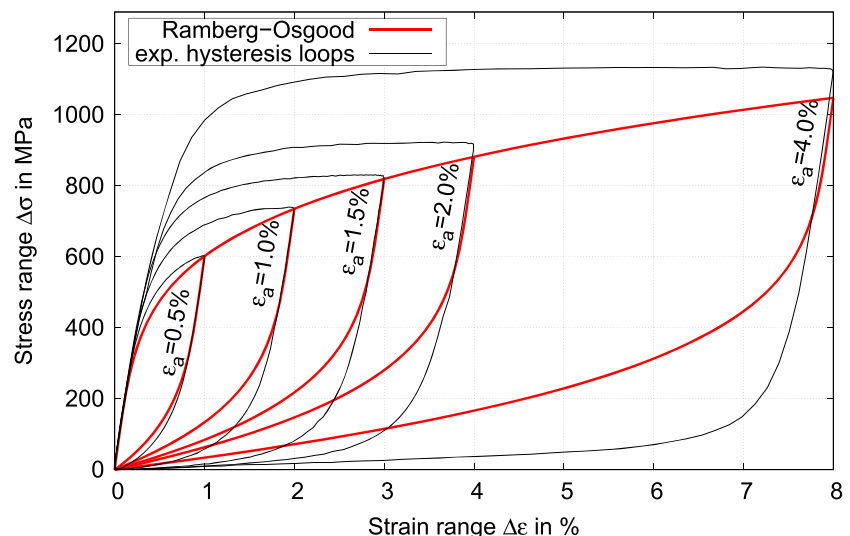
### 2.3 | Constant amplitude loading

Results of strain-controlled constant amplitude loading tests<sup>25</sup> ( $R_e = -1$ ) are in good comparison with data from

literature (e.g., KTA 3201.2<sup>1</sup>), for LCF as well as for HCF. The stress responses at half lifetime ( $N/2$ ) were used to determine the parameters for the cyclic stress–strain curve. The cyclic hardening coefficient and exponent as used in the Ramberg–Osgood<sup>26</sup> equation are  $K' = 1121$  MPa and  $n' = 0.2309$  (temperature is 180°C). Young's modulus was determined at this temperature to  $E = 183000$  MPa. Based on force-controlled constant amplitude loading tests of the hourglass specimens at 180°C, the endurance limit up to a limit load cycle of  $N = 2 \cdot 10^6$  was determined to  $\sigma_D = 214$  MPa using the method of probits.<sup>27</sup> The corresponding strain is  $\epsilon_D = 0.194\%$ .

Due to the process of welding, the heat input up to a temperature of 1200°C for the weld specimens in the HAZ and the simulated HAZ of the Gleeble specimens leads to a recrystallization of the microstructure. As a result of a subsequent slow cooling in air, the grains have more time to grow. The larger grain sizes even affect the strength, resulting in a lower measurable hardness. For the hourglass specimens, the hardness was determined to  $>200$  HV10; for the HAZ of the weld specimens and the Gleeble specimens, the hardness was measured about  $\sim 140$  HV1. In the consequence, the transferability is not given. Therefore, the endurance limit for the Gleeble and Weld specimens was estimated to  $\sigma_D = 160$  MPa.

As observed by the hysteresis loops under constant amplitude loading, the austenitic steel X6CrNiNb18-10 shows a strong non-Masing behavior (see Figure 2). This is also known as ‘‘strain range effect’’<sup>28</sup>; with an increased loading, the material hardens isotropically by an increasing yield strength. Simultaneously, the kinematic plastic deformation behavior equals more and more an ideal plastic behavior at the reversal points. Incremental formulated plasticity models, like the models from Döring<sup>29</sup> and Fang,<sup>30</sup> can describe the evolution of isotropic and



**FIGURE 2** Calculated hysteresis loops with Ramberg–Osgood and Masing behavior in contrast to measured hysteresis loops under constant amplitude loading ( $R_e = -1$ ) at 180°C and half lifetime  $N/2$  for strain ranges. Hysteresis loops were all shifted in the upper reversal point [Colour figure can be viewed at [wileyonlinelibrary.com](http://wileyonlinelibrary.com)]

kinematic hardening. Against the background of the increased effort in processing, this possibility was not further pursued.

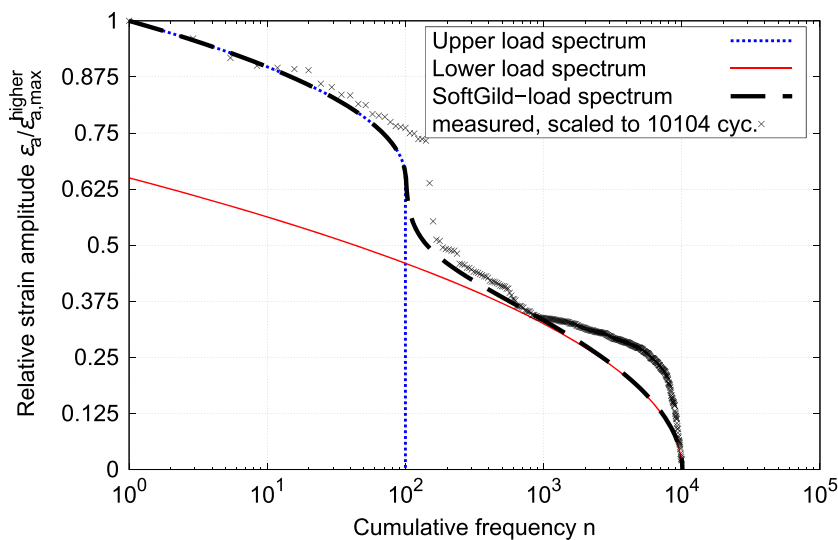
## 2.4 | Variable amplitude loading

In the application relevant here, the variable mechanical load is caused by temperature changes of the medium carried along. Therefore, the operators of such plants monitor the temperature variations over time and calculate the local stress–time histories. Framatome GmbH gave the results of a plant shutdown for a piping at a critical area (welded flange). After rainflow counting, the frequency distribution of the cycles was approximated by superposing two Gaussian-like spectra—sum of two Gaussian-like distributed load spectra (SoftGild). The spectrum contents are 100 cycles for the high-amplitude spectrum and 10 000 cycles otherwise (see Figure 3 and Table 1).

For the experimental investigations by block and pseudorandom loading tests, the spectrum was divided into eight steps, each of the same step size. In the block tests or eight-stage tests, the cycles are run in ascending and descending order, while the individual cycles for the service loading tests are randomized (but with same sequence for each test). Figure 3 shows the spectrum for both the eight stages and the pseudorandom load. The

maximum nominal applied strain amplitude for those tests was chosen to be 0.5% or 0.7%. In some of the pseudorandom load tests of the Gleeble and weld specimens, a thermocycle between 50 and 350°C was superposed. The frequency of the thermocycle is much lower than frequency of the structural loading. One thermocycle corresponds to an average of 112 load cycles for welded specimens and an average of 80 load cycles for Gleeble specimens. In the consequence, the thermal conditions for each mechanical cycle can be seen as isothermal, but over time the thermal condition is non-isothermal. These tests are complemented by two-stage tests at 180°C, where one big cycle is followed by 10, 100, 1000 or 10 000 small cycles. The amplitudes of the latter may be above or below the initial endurance limit. The maximum nominal applied strain amplitude was chosen for HG specimens to be 1.0% and 1.5%, for notched specimen to be 1.0%, and for weld and Gleeble specimens to be 0.5% and 0.7%.

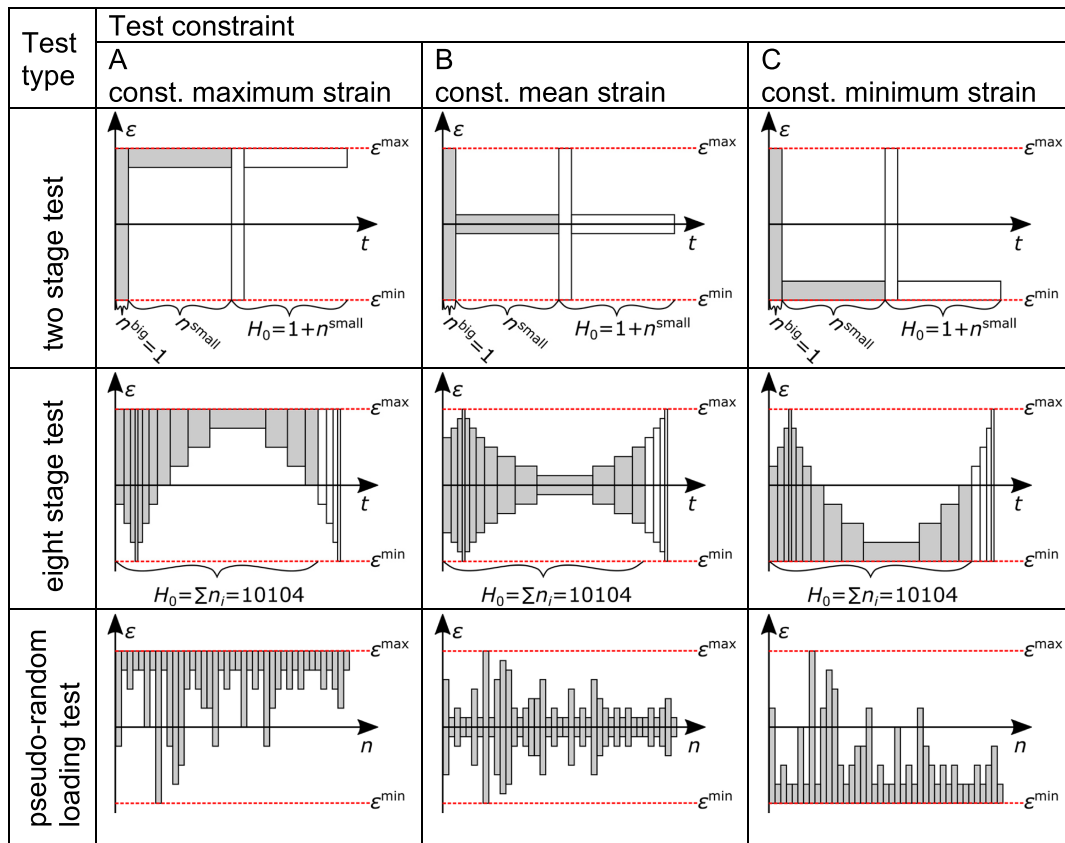
All tests under variable amplitude loadings have in common that the biggest cycles are always performed under a strain ratio of  $R_\epsilon = -1$ . The smaller cycles are hung either at its upper reversal point (Figure 4, Column A) or its lower reversal point (Figure 4, Column C). This leads to high tensile or compressive mean stresses of the small cycles. The positioning on the descending branch of the hysteresis loop of the large cycle under  $R_\epsilon = -1$  (Figure 4, Column B) leads to moderate compressive



**FIGURE 3** Derived load spectra (SoftGild) for strain amplitudes by an upper and a lower load spectrum; sum of those two is compared to measured load spectrum [Colour figure can be viewed at [wileyonlinelibrary.com](http://wileyonlinelibrary.com)]

Step	1	2	3	4	5	6	7	8
Relative amplitude $\epsilon_a/\epsilon_{a,max}$	1	7/8	6/8	5/8	4/8	3/8	2/8	1/8
Frequency	2	8	40	52	42	650	3490	5820
Cumulative frequency	2	10	50	102	144	794	4284	10 104

**TABLE 1** Relative amplitudes and frequencies of each step for derived load spectrum (SoftGild)



**FIGURE 4** Schematic illustration of test matrix with two-stage tests (first line), eight-stage tests (second line), and pseudorandom loading tests (third line); schematic illustration of the pseudorandom loading tests shows just a section of the load spectrum; each bar illustrates one load cycle [Colour figure can be viewed at [wileyonlinelibrary.com](http://wileyonlinelibrary.com)]

mean stresses. A total of 124 variable amplitude loading test results are available for the validation of any life calculation model.

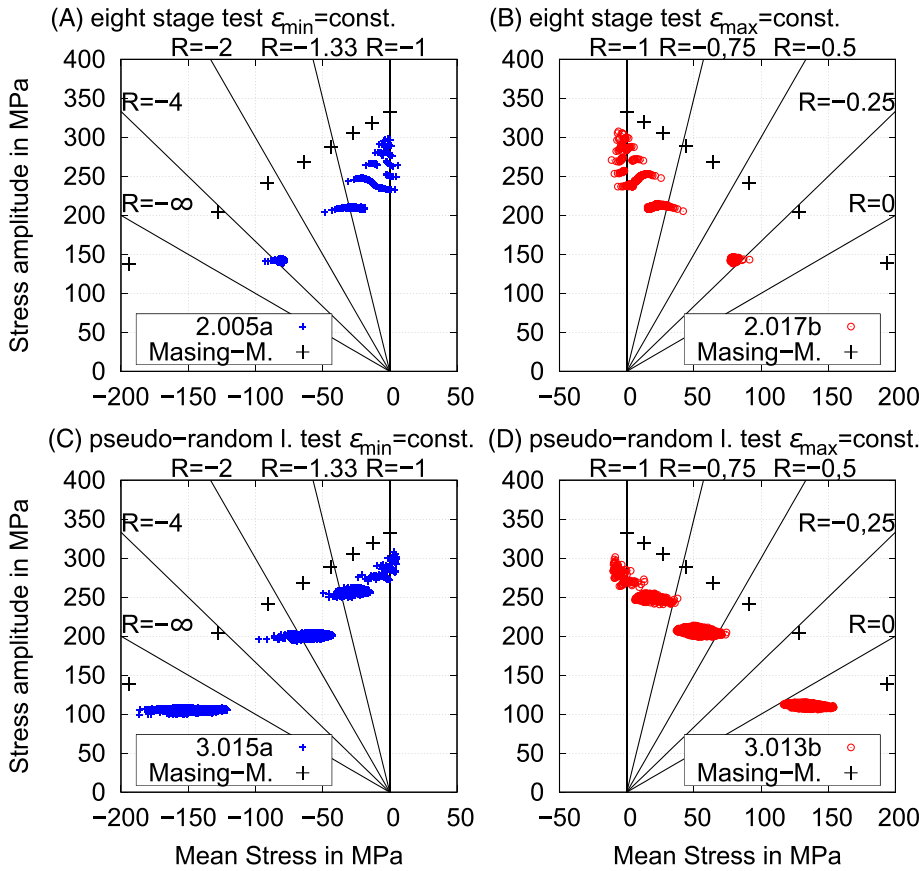
As observed under constant amplitude loading, the strange range effect also occurs under variable amplitude loading. Figure 5 shows a comparison between measured and calculated stress amplitudes over mean stresses for eight-stage and pseudorandom loading tests, each with the condition of constant upper and lower reversal points in strain. Calculations were performed by the Masing-memory behavior with the Ramberg–Osgood law based on the defined load spectra. The experimentally monitored cycles show lower mean stresses as well as lower stress amplitudes than calculated. Deviations through lower stress amplitudes for the highest loadings result mainly by the reversibility of the described strain range effect. Deviations in mean stress result mainly by accumulated mean stress relaxation. Especially with higher plastic deformations, mean stress relaxation is induced. Higher scattering of mean stresses for pseudorandom loading than for the eight-stage tests concerning the lowest amplitude level can be explained by the left variable reversal point of the previous load cycle. Deviations of

too low amplitudes concerning the lowest amplitude under pseudorandom loading are owned by control technology of the servo hydraulic testing machine (deviation between predefined and present strain range).

### 3 | CRACK PROPAGATION MODEL

#### 3.1 | Isothermal fatigue

Describing the metal fatigue phenomenon by modeling crack growth is an ongoing effort for six decades. Numerous researchers have contributed. Again, it is beyond the scope of this paper to give an overview. Only the latest version of a model development started in the early 1990s<sup>12,13</sup> and was revitalized, recently,<sup>17,19,25,31,32</sup> However, it should be noted that the ideas used in the authors' models are not unique. Especially the models of the IWM<sup>33–37</sup> (based on Heitmann's<sup>38,39</sup> damage parameter  $Z_D$ ) follow similar approaches and lead to comparable results. Only the publications of Kamaya and Kawakubo<sup>40</sup> and the school around Topper<sup>41</sup> shall be additionally mentioned here.



**FIGURE 5** Resulting mean stresses measured for HG specimens under variable amplitude strain-controlled loading exemplary for two eight-stage tests and two operational loading tests—In each case one example with constant minimum strain (left) and one example with constant maximum strain (right) compared to calculations with Masing-memory behavior based on stabilized behavior under constant amplitude loading [Colour figure can be viewed at wileyonlinelibrary.com]

Only the variant leading to the best comparison between calculated and experimental fatigue life is presented in this paper: PJ-RifoT2. This variant will be mainly compared in the following to the original  $P_J$ -concept: PJ-Orig<sup>42</sup>. The designations PJ-Orig and PJ-RifoT2 are chosen as in an earlier monograph for reasons of consistency. An approximate solution for the effective cyclic  $J$ -integral is applied according to Dowling<sup>43</sup> for half-circular surface crack in half-space. The damage parameter  $P_J$  considers sequence effects by taking the effective stress and strain ranges into account, which vary depending on the sequence under variable amplitude loading. Another considered sequence effect depends on the crack length, caused by the decreasing fatigue strength with increasing crack length. The transition from short crack growth to long crack growth is only considered by the threshold behavior; the additional higher crack growth rate of short cracks is considered integrally over the whole fatigue life. The developed concept variant PJ-RifoT2 differs from PJ-Orig at first by the crack propagation law:

$$\frac{da}{dn} = \begin{cases} C_J \cdot (\Delta J_{eff})^{m_J} & \text{for } \Delta J_{eff} \geq \Delta J_{eff,th} \quad \text{PJ-Orig} \\ C_J \cdot ((\Delta J_{eff})^{m_J} - (\Delta J_{eff,th})^{m_J}) & \text{for } \Delta J_{eff} \geq \Delta J_{eff,th} \quad \text{PJ-RifoT2} \end{cases} \quad (1)$$

$$\frac{da}{dn} = \begin{cases} C_J \cdot (\Delta J_{eff})^{m_J} & \text{for } \Delta J_{eff} \geq \Delta J_{eff,th} \quad \text{PJ-Orig} \\ C_J \cdot ((\Delta J_{eff})^{m_J} - (\Delta J_{eff,th})^{m_J}) & \text{for } \Delta J_{eff} \geq \Delta J_{eff,th} \quad \text{PJ-RifoT2} \end{cases} \quad (2)$$

Equation (2) can be integrated analytically with  $P_J = \Delta J_{eff}/a = \text{const.}$  from initial crack length  $a_0$  to crack length at failure  $a_{end}$ :

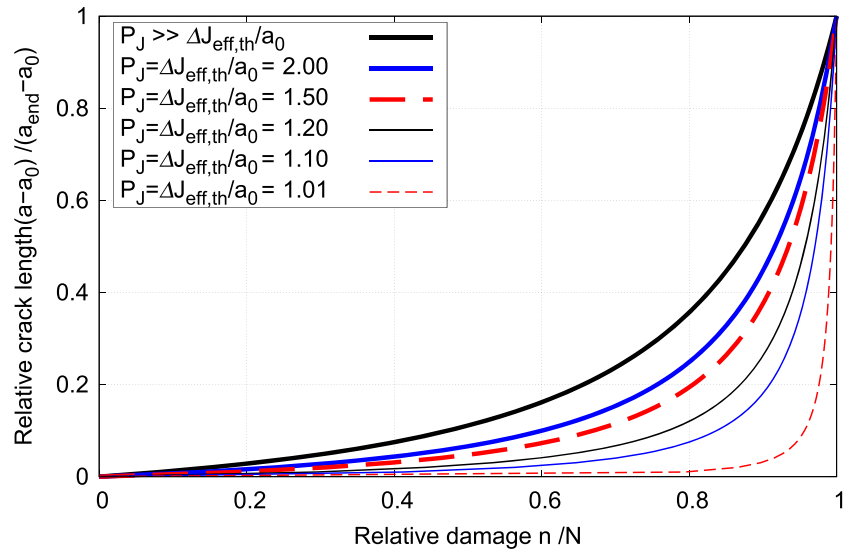
$$N = \frac{(a_{end})^{1-m_J} - (a_0)^{1-m_J}}{(1-m_J) \cdot C_J} \cdot (P_J)^{-m_J} \quad (4)$$

This leads to an explicit relation between actual crack length  $a$  and relative damage  $n/N$  by

$$n/N = \frac{(a)^{1-m_J} - (a_0)^{1-m_J}}{(a_{end})^{1-m_J} - (a_0)^{1-m_J}} \quad (5)$$

Based on this relation, in the original  $P_J$ -concept a linear damage accumulation is performed rather than a crack growth calculation. Using Equation (3), a crack growth calculation has to be performed for PJ-RifoT2 instead of a linear damage accumulation, and the crack growth rate is a function of the effective cyclic  $J$ -integral. Considering the threshold value  $\Delta J_{eff,th}$  in the crack growth law results in a load-dependent behavior for relation between crack length and relative damage  $n/N$  under constant amplitude loading (see Figure 6). This requires an improved

**FIGURE 6** Relation between relative crack length and relative damage under constant amplitude loading and the assumption of stabilized crack closure behavior depending on load level relative to threshold [Colour figure can be viewed at wileyonlinelibrary.com]



approach to identify the crack growth parameters  $C_J$  and  $m_J$  based on constant amplitude loading tests. Therefore, only fatigue tests were considered, where the influence of the threshold value  $\Delta J_{eff,th}$  is neglectable:  $P_J = \Delta J_{eff}/a \gg \Delta J_{eff,th}/a$ . Only tests with lifetimes lower than 10 000 cycles were chosen. For this case, Equation (3) can be treated as Equation (2), with the benefit to calculate the fatigue life analytically according to Equation 4. To consider the threshold behavior of short cracks similarly as El Haddad<sup>44</sup> or Tanaka,<sup>45</sup> the integration limits are to be extended by the microstructural length  $l^*$ :

$$N = \frac{((a_{end} + l^*)^{1-m_J} - (a_0 + l^*)^{1-m_J})}{(1-m_J) \cdot C_J} \cdot (P_J)^{-m_J} = Q \cdot (P_J)^{-m_J} \tag{6}$$

For the identification of the parameter  $Q$  and the crack growth exponent  $m_J$ , a  $P_J$ -Wöhler curve needs to be fitted by a linear regression to the pairs of lifetimes  $N$  (<10000 cyc.) and  $P_J$  with:

$$P_J = \frac{\Delta J_{eff}}{a} = \left[ 1.24 \frac{\Delta \sigma_{eff}^2}{E} + \frac{1.02}{\sqrt{n'}} \Delta \sigma_{eff} \cdot \left( \Delta \varepsilon_{eff} - \frac{\Delta \sigma_{eff}}{E} \right) \right] \tag{7}$$

Therefore, the effective stress and strain ranges  $\Delta \sigma_{eff}$  and  $\Delta \varepsilon_{eff}$  are calculated between the difference of the upper reversal point of the hysteresis loop and the point of crack closure:

$$\Delta \sigma_{eff} = \sigma_{max} - \sigma_{cl} \tag{8}$$

$$\Delta \varepsilon_{eff} = \varepsilon_{max} - \varepsilon_{cl} \tag{9}$$

The crack opening stress is calculated according to Newman's model<sup>46</sup>:

$$\frac{\sigma_{op}}{\sigma_{max}} = \begin{cases} A_0 + A_1 \cdot R + A_2 \cdot R^2 + A_3 \cdot R^3 & \text{for } R \geq 0 \\ A_0 + A_1 \cdot R & \text{for } -2 < R < 0 \\ A_0 - 2 \cdot A_1 & \text{for } R \leq -2 \end{cases} \tag{10}$$

with

$$A_0 = 0.535 \cos\left(\frac{\pi \cdot \sigma_{max}}{2 \cdot \sigma_0}\right),$$

$$A_1 = 0.344 \frac{\sigma_{max}}{\sigma_0},$$

$$A_2 = 1 - A_0 - A_1 - A_3,$$

$$A_3 = 2A_0 + A_1 - 1,$$

$$\sigma_0 = \frac{R_m + R'_{p0.2}}{2}.$$

Under the assumption that the crack opening strain is equal to the crack closure strain  $\varepsilon_{op} = \varepsilon_{cl}$ , crack closure strain as well as crack closure stress can be determined by Ramberg–Osgood equation. With the identified parameter  $Q$  and the crack growth exponent  $m_J$ , the additional parameters like the initial crack length  $a_0$  and the microstructural length  $l^*$  as well as the crack growth constant  $C_J$  can now be identified. At this step, the additional consideration of transient crack closure plays an



important role as an improvement in contrast to the original  $P_J$ -concept. Under constant amplitude loading, the original  $P_J$ -concept uses a constant stabilized crack closure strain independent from crack length. Transient crack closure means that the crack closure stress develops with the increasing crack length under constant amplitude loading, too. With this additional component in the concept, the fact is taken into account that the stabilized level of plasticity-induced crack closure still has to be formed. At the beginning of crack initiation by forming slip bands, the crack grows along those slip bands in a direction of  $45^\circ$  to the loading as a shear crack (Stage I).<sup>47,48</sup> At this state, growth of those cracks is very sensitive to microstructure by grain boundaries, triple points, and phase boundaries.<sup>49–51</sup> During shear crack growth, no plasticity-induced crack closure effects are active, and the whole cycle of each hysteresis loop is fully damaging.<sup>15</sup> The crack closure effect only sets in with the transition to Mode I crack propagation (Stage II) at higher stresses and/or longer cracks. The influence of transient crack closure on the effective stress and strain ranges is very important in the HCF regime. In the LCF regime, the effective stress and strain ranges are approximately equal to the full stress and strain ranges, so  $P_J = \text{const.}$  under constant amplitude loading and Equation 4 can still be used. The transient crack closure strain is formulated under the conditions of constant amplitude loadings by

$$\varepsilon_{\text{cl, const}}^a = \varepsilon_{\text{cl, const}} - (\varepsilon_{\text{cl, const}} - \varepsilon_{\text{min}}) \cdot \exp((a - a_0)/\Delta a_{\text{ref}}). \quad (11)$$

The delay constant  $\Delta a_{\text{ref}}$  is not only used for modeling the transient crack closure behavior. Anthes<sup>15</sup> showed that under variable amplitude loading, the transition between a current crack closure strain  $\varepsilon_{\text{cl}}$  and a stabilized crack closure strain  $\varepsilon_{\text{cl, const}}^a$  can be expressed in the same way:

$$\varepsilon_{\text{cl, new}} = \varepsilon_{\text{cl, const}}^a - (\varepsilon_{\text{cl, const}}^a - \varepsilon_{\text{cl}}) \cdot \exp(-\Delta a/\Delta a_{\text{ref}}). \quad (12)$$

Anthes<sup>15</sup> describes his delay parameter according to Gamache and McEvily<sup>52</sup> as inversely proportional to the ultimate tensile strength  $R_m$  by

$$\Delta a_{\text{ref}} = \frac{\text{MPa} \cdot \text{mm}}{R_m} \cdot \frac{872}{90}. \quad (13)$$

The difference between damage contributions according to older (PJ-Orig) and updated crack incrementally controlled delay (PJ-RifoT2) is shown for an example of a

two-stage test in Figure 7. In the older version, the delay occurs identically in each run through the load spectrum. Based on crack length controlled delay, in the first runs through the load spectra, the effective strain ranges of the smaller cycles are not reduced, and their amplitudes are damaging with their full range. Only with a higher crack length and longer crack increments can the crack opening strain exceed minimum strain of the individual cycles. Vormwald as well as Anthes used for evaluation of their delay constant. The delay constant  $\Delta a_{\text{ref}}$  was derived by theoretical considerations and validations<sup>19</sup> using prestrain Wöhler curves from Heuler<sup>53</sup>:

$$\Delta a_{\text{ref}} = \left( \frac{38.8 \text{MPa}}{R_m} \cdot \left( (0.25 \text{mm} + a_0^* - a_0)^{1-m_1} - (a_0^*)^{1-m_1} \right) + (a_0^*)^{1-m_1} \right)^{\frac{1}{1-m_1}} - a_0^* \quad (14)$$

with

$$a_0^* = \frac{\Delta J_{\text{eff, th}}}{P_{J, D}^{a=a_0}}. \quad (15)$$

Therefore,  $P_{J, D}^{a=a_0}$  denotes the initial value for the  $P_J$  parameter at the level of the endurance limit, calculated by the full stress and strain ranges  $\Delta \sigma_D$  and  $\Delta \varepsilon_D$ :

$$P_{J, D}^{a=a_0} = \left[ 1.24 \frac{\Delta \sigma_D^2}{E} + \frac{1.02}{\sqrt{n'}} \Delta \sigma_D \cdot \left( \Delta \varepsilon_D - \frac{\Delta \sigma_D}{E} \right) \right], \quad (16)$$

while the threshold of the effective cyclic  $J$ -integral  $\Delta J_{\text{eff, th}}$  is kept independent from R-ratio and is approximately calculated by Young's modulus based on data from Taylor<sup>54</sup> with

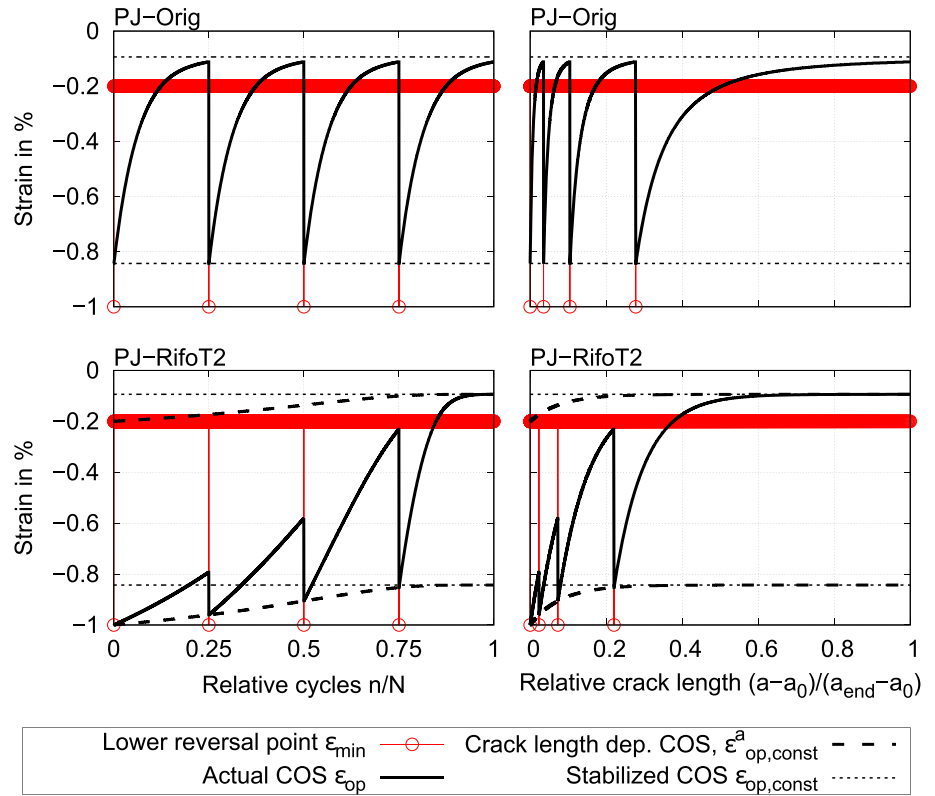
$$\Delta J_{\text{eff, th}} = \frac{E}{5 \cdot 10^6} \text{mm}. \quad (17)$$

The presented effective threshold is to be interpreted as an intrinsic value. The proposed delay constant, Equation 14, yields much smaller values than proposed by Anthes, Equation 13. The consequences on calculated fatigue lives will be shown later. For high values of the delay constant  $\Delta a_{\text{ref}}$ , the microstructural crack length is determined depending on the defined initial crack length  $a_0$  by

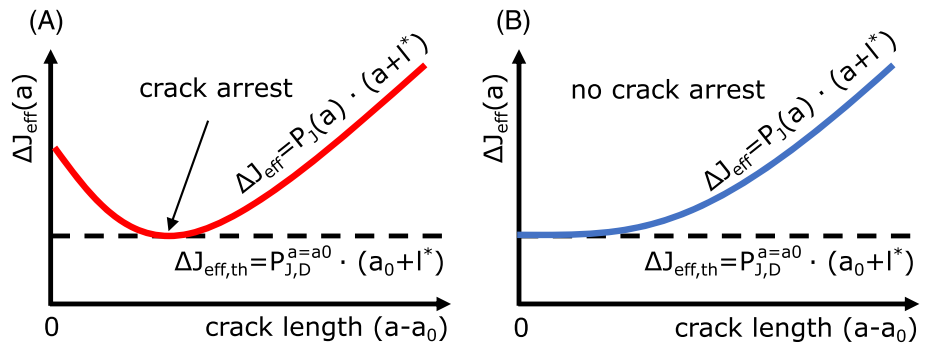
$$l^* = a_0^* - a_0 = \frac{\Delta J_{\text{eff, th}}}{P_{J, D}^{a=a_0}} - a_0. \quad (18)$$

Especially for small values of the delay constant, crack arrest occurs (see Figure 8a). For this case, the microstructural length  $l^*$  needs to be determined iteratively, in the way that the minimum value of the crack length-

**FIGURE 7** Schematic behavior of crack closure strain (COS) for concept PJ-Orig and PJ-RifoT2 for an exemplary two-stage test (one cycle with  $\epsilon_a = 1\%$  under  $R_\epsilon = -1$  followed by a high number of cycles with  $\epsilon_a = 0.2\%$  under  $R_\epsilon = -1$ ) normalized to four repeats, shown over relative cycles (left column) and relative crack length (right column) [Colour figure can be viewed at wileyonlinelibrary.com]



**FIGURE 8** Example for crack arrest (a) and no crack arrest (b) [Colour figure can be viewed at wileyonlinelibrary.com]



dependent effective cyclic  $J$ -integral is equal to the threshold value by the variation of crack length  $a$  in the ranges of  $a_0$  and  $a_{end}$ :

$$0 = P_J(a, \sigma_D, \Delta a_{ref}) \cdot (a + l^*) - \Delta J_{eff,th}, \quad a \in [a_0, a_{end}]. \quad (19)$$

With the identified microstructural length, the delay constant does not need to be estimated for a second time; however, the crack growth constant  $C_J$  is calculated finally by

$$C_J = \frac{(a_{end} + l^*)^{1-m_J} - (a_0 + l^*)^{1-m_J}}{(1-m_J) \cdot Q}. \quad (20)$$

With this step, all parameters are identified to calculate lives under variable amplitude loadings. The input to the algorithm is given by identified hysteresis loops of local stress and strain histories. For cases of local stress concentration, the local stress strain path has to be calculated under consideration of the effective stress concentration factor  $K_f$ . The procedure consists of the following steps:

1. Calculation of the stabilized crack opening stress according to Newman<sup>46</sup> including modifications<sup>55</sup> for given maximum stress  $\sigma_{max}$  and stress based R-ratio for each load cycle individually, according to Equation 10.
2. Calculation of the stabilized crack opening/closure strain under constant amplitude loading:

$$\varepsilon_{op,const} = \varepsilon_{cl,const} = \varepsilon_{min} + \frac{\sigma_{op} - \sigma_{min}}{E} + 2 \left( \frac{\sigma_{op} - \sigma_{min}}{2 \cdot K'} \right)^{\frac{1}{n'}} \quad (21)$$

2a. Calculation of the crack length-dependent crack opening/closure strain:

$$\varepsilon_{op,const}^a = \varepsilon_{cl,const} - (\varepsilon_{cl,const} - \varepsilon_{min}) \cdot \exp((a - a_0)/\Delta a_{ref}) \quad (22)$$

Store  $\varepsilon_{op,const}^a$  as  $\varepsilon_{op,const}$ .

3. Calculation of the crack opening strain for the actual cycle  $\varepsilon_{op}$  depending on the crack opening strain of the previous cycle  $\varepsilon_{op,prev}$ :

Special cases:

For  $\varepsilon_{max} > \varepsilon_{max,old}$  OR  $\varepsilon_{min} < \varepsilon_{min,old} \rightarrow \varepsilon_{op} = \varepsilon_{op,const}$

For  $\varepsilon_{max} \leq \varepsilon_{op,prev} \rightarrow \varepsilon_{op} = \varepsilon_{op,prev}$

Cases with  $\varepsilon_{op,const} \geq \varepsilon_{op,prev} \rightarrow \varepsilon_{op} = \varepsilon_{op,prev}$ .

Cases with  $\varepsilon_{op,const} < \varepsilon_{op,prev}$

For  $\sigma_a \geq 0.4 \sigma_0 \rightarrow \varepsilon_{op} = \varepsilon_{op,const}$

For  $\sigma_a < 0.4 \sigma_0 \rightarrow \varepsilon_{op} = \varepsilon_{op,prev}$

4. Calculation of the crack closure stress:

For  $\varepsilon_{op} \leq \varepsilon_{min} \rightarrow \sigma_{cl} = \sigma_{min}$

For  $\varepsilon_{op} > \varepsilon_{min}$ , iterative determination of crack closure stress:

$$0 = \varepsilon_{max} - \varepsilon_{op} - \frac{\sigma_{max} - \sigma_{cl}}{E} - 2 \left( \frac{\sigma_{max} - \sigma_{cl}}{2 \cdot K'} \right)^{\frac{1}{n'}} \quad (23)$$

5. Calculation of the effective cyclic J-integral:

$$\Delta J_{eff} = \left[ 1.24 \frac{\Delta \sigma_{eff}^2}{E} + \frac{1.02}{\sqrt{n'}} \Delta \sigma_{eff} \cdot \left( \Delta \varepsilon_{eff} - \frac{\Delta \sigma_{eff}}{E} \right) \right] \cdot (a + l^*) \quad (24)$$

with

$$\Delta \sigma_{eff} = (\sigma_{max} - \sigma_{cl})$$

$$\Delta \varepsilon_{eff} = (\varepsilon_{max} - \varepsilon_{op})$$

6. Calculation of the crack length increment  $\Delta a$  and the new crack length  $a_{new}$ :

$$\Delta a = \begin{cases} C_J \cdot ((\Delta J_{eff})^{m_{J1}} - (\Delta J_{eff,th})^{m_{J1}}) & \text{for } \Delta J_{eff} \geq \Delta J_{eff,th} \\ 0 & \text{for } \Delta J_{eff} < \Delta J_{eff,th} \end{cases} \quad (25)$$

$$a_{new} = a + \Delta a \quad (26)$$

7. Calculation of the left level of the crack opening strain for the next cycle, based on the stabilized crack opening strain  $\varepsilon_{op,const}$ , the crack opening strain used for the calculation of the actual  $P_J$ -value, and the crack length increment  $\Delta a$ :

$$\varepsilon_{op,new} = \varepsilon_{op,const} - (\varepsilon_{op,const} - \varepsilon_{op}) \cdot \exp(-\Delta a/\Delta a_{ref}) \quad (27)$$

8. For the next cycle, the following parameters have to be checked or replaced:

If  $\varepsilon_{max} > \varepsilon_{max,old} \rightarrow \varepsilon_{max,old} = \varepsilon_{max}$

If  $\varepsilon_{min} < \varepsilon_{min,old} \rightarrow \varepsilon_{min,old} = \varepsilon_{min}$

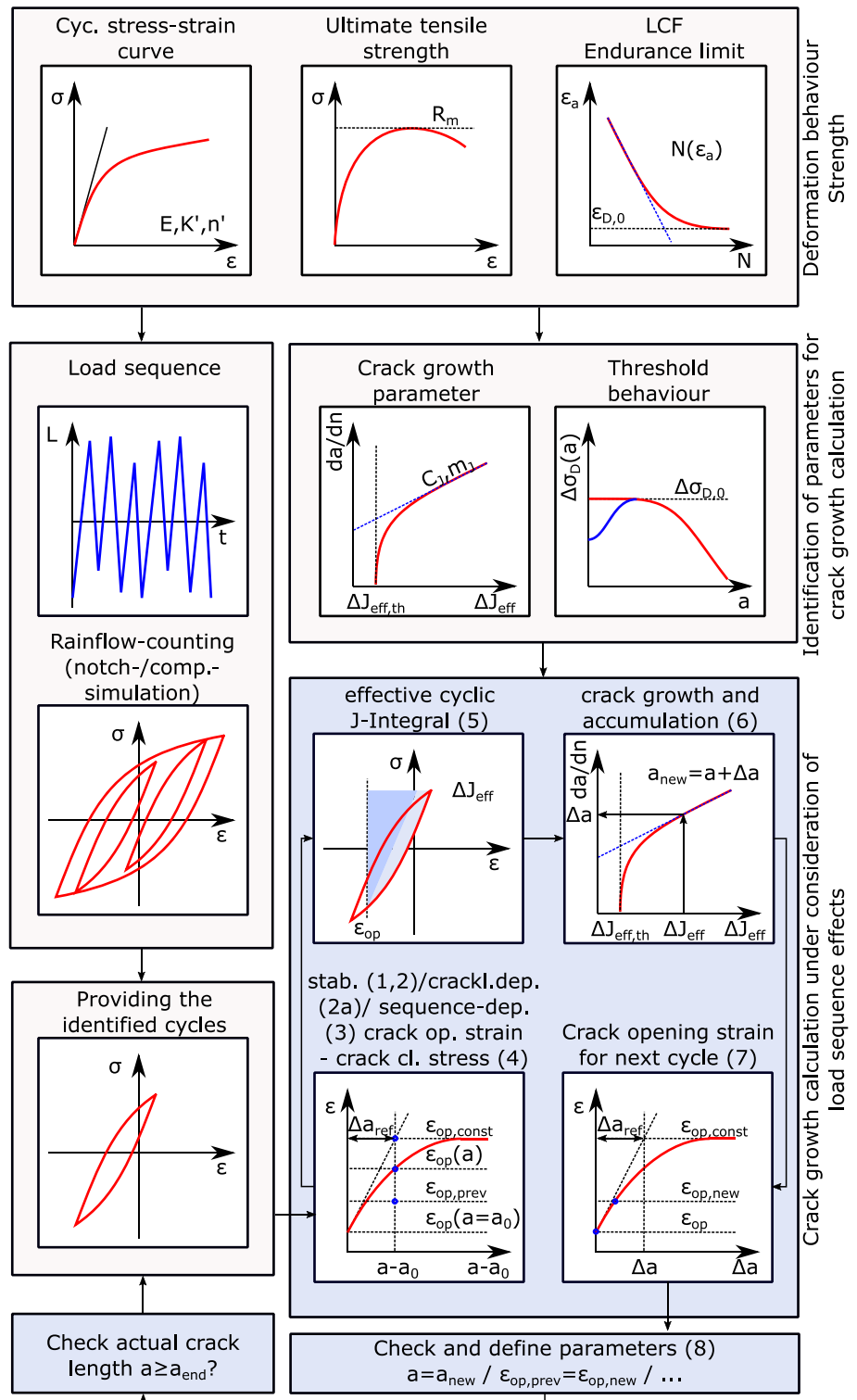
and

$$a = a_{new}$$

$$\varepsilon_{op,prev} = \varepsilon_{op,new}$$

Steps 1–8 are repeated until the crack length reaches the defined criteria for the technical crack length:  $a \geq a_{end}$ . An overview is given in Figure 9.

**FIGURE 9** Overview of the presented procedure for input and identification of parameters, providing the load input and how to perform under variable amplitude loading [Colour figure can be viewed at wileyonlinelibrary.com]



### 3.2 | Variable temperature

Under an additional loading by variable temperatures, the crack growth parameters have to be identified for some temperatures. Under the assumption that the change of temperature for one cycle is small (e.g.,  $\Delta T < 10K$ ), the mean temperature of each cycle can

be taken for the damage calculation. For the range between ambient temperature and  $350^\circ C$ , the strain life curves of the material under investigation differ only in the HCF region. Depending on this constraint and the relation given by Equation 7, the following expression describes the relation between the crack growth exponent  $m_j$  and the Ramberg–Osgood exponent  $n'$ :

$$m_J(T) \cdot (1 + n'(T)) = \text{const.} \quad (28)$$

The crack growth exponent for a given Temperature  $T$  depends on the Ramberg–Osgood exponent and the corresponding values for a reference temperature  $T_{\text{ref}}$ :

$$m_J(T) = m_J(T_{\text{ref}}) \cdot \frac{(1 + n'(T_{\text{ref}}))}{(1 + n'(T))}. \quad (29)$$

For the coefficient  $Q(T) \cdot (P_J(T, \varepsilon_a))^{-m_J(T)} = \text{const.}$ , the same condition leads to

$$Q(T) = Q(T_{\text{ref}}) \cdot \frac{(P_J(T_{\text{ref}}, \varepsilon_a))^{-m_J(T_{\text{ref}})}}{(P_J(T, \varepsilon_a))^{-m_J(T)}}. \quad (30)$$

These relations are derived for cycles with high stress and strain ranges where these ranges are nearly similar to effective stress and strain ranges. The crack growth constant  $C_J$  and the microstructural length  $l^*$  have to be identified in the same way as under constant temperature. A constant value for the chosen initial crack length  $a_0$  is the only condition which need to be fulfilled.

The damage parameter  $D_{\text{TMF}}^{33-37}$  calculated with temperature-dependent material parameters uses an effective cyclic  $J$ -integral related to crack length and temperature-dependent value of  $R'_{p0.1}$ . Within this concept, crack growth coefficient and crack growth exponent keep constant. For the damage parameter  $P_J$  calculated with temperature-dependent material parameters, this kind of temperature dependency can easily be done by

$$P_J(T_{\text{ref}}) = P_J(T) \cdot \frac{R'_{p0.1}(T_{\text{ref}})}{R'_{p0.1}(T)}. \quad (31)$$

This approach was used to make PJ-Orig temperature dependent. Used parameters of resistance side were taken from reference temperature  $T_{\text{ref}}$ . This led to the consequence of inconsistencies in strain Wöhler curves and endurance limits in contrast to experimental values. Based on those observations, the temperature dependency for PJ-RifoT2 was motivated to avoid those inconsistencies and performed as shown above.

## 4 | PARAMETER IDENTIFICATION

### 4.1 | PJ-based concepts

The parameters are presented in Table 2. Resulting strain Wöhler curves for both concepts are compared to results

under constant amplitude loadings in Figure 10. Differences of the crack growth exponent lead to different slopes of strain Wöhler curves. For calculations under variable temperature, with temperatures above and below 180°C, two additional supporting points were added at 20 and 350°C. For these temperatures, Ramberg–Osgood parameters were estimated following previous investigations.<sup>56</sup> The endurance limit was estimated as  $\sigma_D = 0.43 \cdot R_m$  where the factor 0.43 is the same at 180°C. Table 1 shows two parameter sets for PJ-RifoT2. The first one bases on the delay constant published by Anthes<sup>15</sup> (Equation 13), and the second one (Equation 14) bases on the work of the author.<sup>19</sup> For the second, crack arrest occurs.

### 4.2 | Further concepts

In addition to calculations with PJ-Orig and PJ-RifoT2, calculations with models based on the damage parameter  $Z_D^{38}$  were performed.<sup>19</sup> Some codes, for example, KTA 3201.2<sup>1,57</sup> or the ASME Code Section VIII,<sup>2</sup> use only Wöhler curves for strain ranges without considering load sequence and mean stress effects. Therefore, calculation results are presented for comparison based on the strain life curve of Langer<sup>58</sup> or according to the equation of Manson–Coffin<sup>59,60</sup> and Basquin<sup>61</sup> proposed by Morrow<sup>62</sup>:

$$\varepsilon_a = \varepsilon_a^{\text{el}} + \varepsilon_a^{\text{pl}} = \frac{\sigma'_f}{E} \cdot (2 \cdot N)^b + \varepsilon'_f \cdot (2 \cdot N)^c. \quad (32)$$

Compatibility conditions with the Ramberg–Osgood parameters are considered:

$$n' = \frac{b}{c}, \quad (33)$$

$$K' = \frac{\sigma'_f}{(\varepsilon'_f)^{n'}}. \quad (34)$$

A further possibility based on this description is to consider the mean stress according to Smith, Watson, and Topper<sup>63</sup>: Within the FKM guideline nonlinear,<sup>11</sup> a modified Smith–Watson–Topper damage parameter is used by the work of Bergmann<sup>64</sup> taking the mean stress sensitivity into account. Both damage parameters

$$P_{\text{SWT}} = \sqrt{(\sigma_a + \sigma_m) \cdot \varepsilon_a \cdot E} \text{ for Smith – Watson – Topper,} \quad (35)$$

TABLE 2 Material parameters for X6CrNiNb18-10 at temperature of 180°C

Results of materials tests						
Temp. $T$ in °C	Young's modulus $E$ in °C	Hardening coeff. $K'$ in °C	Hardening exp. $n'$ in °C	Ultimate tensile strength $R_m$ in MPa	Endurance limit* $\sigma_D$ in MPa	Threshold value $\Delta J_{eff,th}$ in MPa mm
20	199 182	2018	0.2969	675	290	0.0398
180	183 000	1,121	0.2309	495	214	0.0366
350	172 410	793	0.1941	440	190	0.0345

Derived model-dependent parameters <sup>a</sup> valid for HG, smooth and notched specimens, $a_{end} = 0.25$ mm, indirect parameters in brackets						
Model	Parameters					
PJ-Orig	$m_j - C_j$ in <sup>b</sup>	$Q$ in cyc./ $(MPa^{-m_j})$	$l^*$ in mm	$a_0$ in mm	$P_{J,D,0}$ in MPa	
	1.863 0.0000650	509 588	0.0133	0.0181	1.167	
PJ-RifoT2 based on Equation 13 with $\Delta a_{ref} = 0.0196$ mm	$m_j - C_j$ in <sup>b</sup>	$(Q)$ in cyc./ $(MPa^{-m_j})$	$l^*$ in mm	$a_0$ in mm	$P_{J,D}^{a=a_0}$ in MPa	
	1.589 0.0000913	188 903	0.0139	0.0	2.636	
PJ-RifoT2 based on Equation 14 with $\Delta a_{ref} = 0.0017$ mm	$m_j - C_j$ in <sup>b</sup>	$(Q)$ in cyc./ $(MPa^{-m_j})$	$l^*$ in mm	$a_0$ in mm	$P_{J,D}^{a=a_0}$ in MPa	
	1.589 0.0000603	188 903	0.0247	0.0	2.636	

Parameters for describing the strain life curve and the mean stress sensitivity				
Model	Parameters			
Manson–Coffin and Basquin (MCB), Smith–Watson–Topper (SWT) and Bergmann	$\sigma'_f$ in MPa	$\epsilon'_f -$	$b -$	$c -$
	764	0.19025	-0.09391	-4.0671
Bergmann	$k$ for $\sigma_m \geq 0$	$k$ for $\sigma_m < 0$		
	0.1519	0.0494		

<sup>a</sup>Reduced endurance limit for weld and Gleeble specimens (see chapter 2.3).

<sup>b</sup>Unit for  $C_j$ : mm/(cyc. [N/mm] <sup>$m_j$</sup> ).

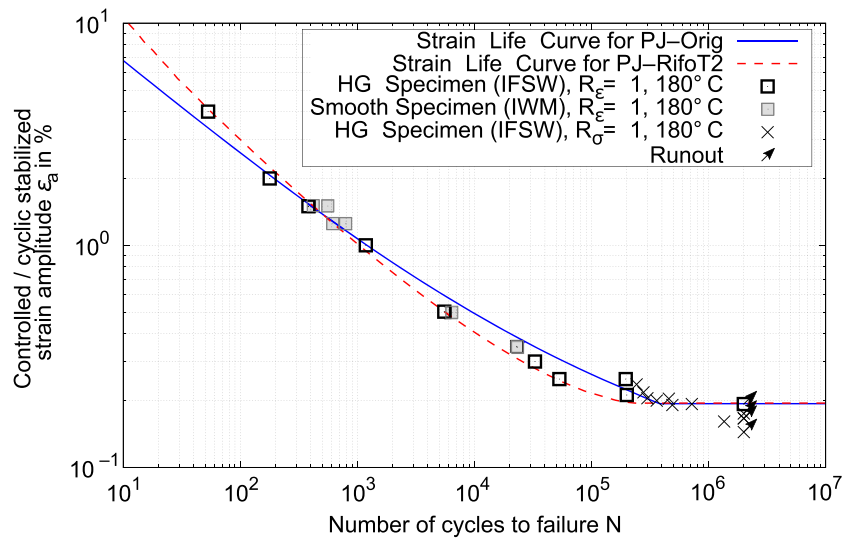


FIGURE 10 Comparison of resulting strain life curves under constant amplitude loading for PJ-Orig and with improved adjustment for PJ-RifoT2 in contrast to experimental results for HG- and smooth specimens [Colour figure can be viewed at wileyonlinelibrary.com]

$$P_B = \sqrt{(\sigma_a + \sigma_m \cdot k) \cdot \varepsilon_a \cdot E} \text{ for Bergmann,} \quad (36)$$

share same damage parameter Wöhler curve:

$$P_{\text{SWT}} = P_B = \sqrt{\sigma'_f \cdot (2 \cdot N)^{2 \cdot b} + \sigma'_f \cdot \varepsilon'_f \cdot E \cdot (2 \cdot N)^{b+c}}. \quad (37)$$

The derived parameters for this Wöhler curve are given in Table 1 as well as the used Bergmann parameter  $k$  distinguishing between positive and negative mean stress as in the FKM guideline nonlinear.<sup>11</sup> For calculations of fatigue lives of tests under variable amplitude loading, the life curves of 180°C were used. No endurance limit was specified when applying Equation 32 or 36.

## 5 | RESULTS

Calculated fatigue lives in contrast to the experimentally ones are shown in Table 3. All 124 tests under variable amplitude loading were statistically evaluated using the estimated probability by Rossow.<sup>65</sup> Using this method, all ratios of numerical calculated results to experimental

results by  $N_{\text{num}}/N_{\text{exp}}$  were calculated and sorted in ascending order. Based on this order, the probabilities were assigned subsequently. The statistical values include the mean value  $P_{50\%}$ , the scattering  $1/T_{10\%/90\%}$  by ratio of probability values of 90%–10%, and the minimum and maximum values and their scattering. Calculations based on three different kinds of input data:

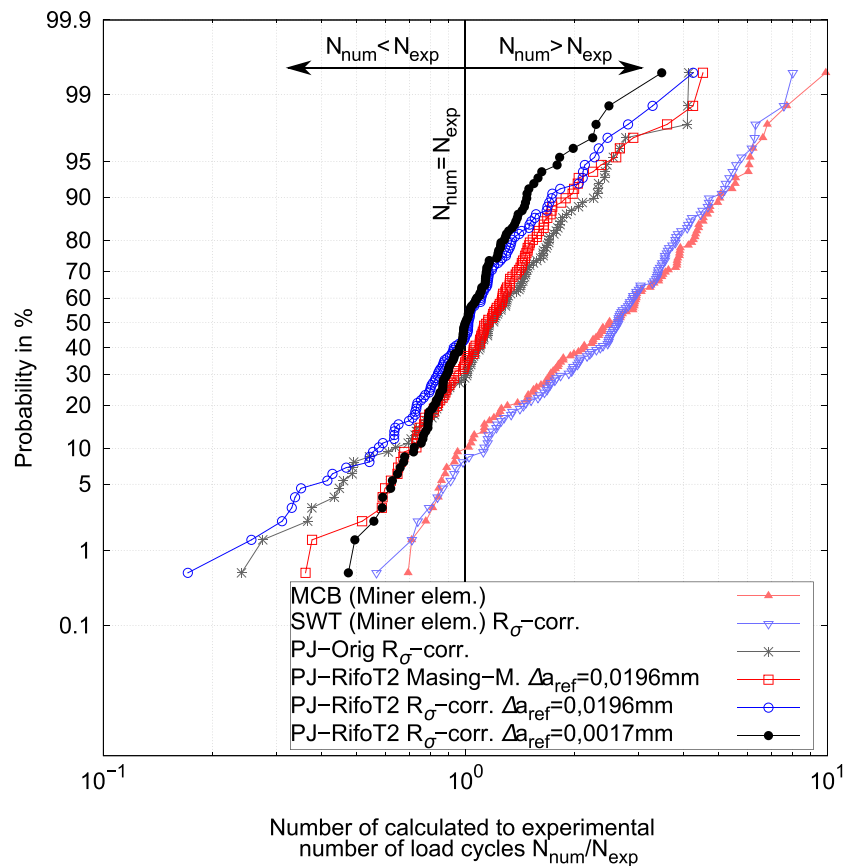
1. Predefined strain histories,
2. Applied strain histories including deviations by control of servo hydraulic testing machine based on one representative load spectrum at half lifetime,
3. Applied load histories including deviations by control of servo hydraulic testing machine and relative correction of mean stresses by measurements (including cyclic plastic deformation behavior) of the material based on one representative load spectrum at half lifetime; for notch and weld specimens, nominal stress histories were taken.

Figure 11 includes a selection of the last two possibilities of input data. In total, the  $P_J$ -based concepts show a higher quality of the prediction with increasing accuracy of the input data. This is not observed for the calculations

**TABLE 3** Comparison of calculated and experimentally achieved fatigue lives based on statistical values for several models and type of input data

Model	Input	$P_{50\%}$	$1/T_{10\%/90\%}$	min	max	max/min
MCB	Predefined strain histories	2.51	4.78	0.65	8.86	13.63
SWT		2.39	8.73	0.19	35.9	188.58
Bergmann		2.35	3.8	0.69	7.66	11.14
PJ-Orig		1.20	3.32	0.21	4.62	21.75
PJ-RifoT2		1.07	2.84	0.25	4.70	18.50
$\Delta a_{\text{ref}} = 0.0196 \text{ mm}$						
MCB	Applied strain histories	2.48	4.97	0.69	9.87	14.22
SWT		2.14	7.08	0.39	37.07	94.52
Bergmann		2.51	4.01	0.70	8.61	12.38
PJ-Orig		1.26	2.98	0.28	7.48	26.99
PJ-RifoT2		1.08	2.66	0.36	4.53	12.52
$\Delta a_{\text{ref}} = 0.0196 \text{ mm}$						
MCB	Applied strain histories, $R_c$ -corrected	2.43	5.24	0.53	10.43	19.88
SWT		2.64	4.17	0.57	8.02	14.13
Bergmann		2.45	4.58	0.55	9.48	17.18
PJ-Orig		1.16	3.51	0.24	4.14	17.19
PJ-RifoT2		0.99	2.75	0.17	4.26	25.00
$\Delta a_{\text{ref}} = 0.0196 \text{ mm}$						
PJ-RifoT2		1.00	2.04	0.48	3.49	7.34
$\Delta a_{\text{ref}} = 0.0017 \text{ mm}$						

**FIGURE 11** Comparison of different damage concepts and variations concerning quality of lifetime prediction [Colour figure can be viewed at [wileyonlinelibrary.com](http://wileyonlinelibrary.com)]



based on strain ranges by Manson–Coffin and Basquin (MCB) and Smith–Watson–Topper (SWT) or the damage parameter by Bergmann. Best results are achieved in this group by the damage parameter of Bergmann followed by the consideration of pure strain ranges with MCB. In average, these calculations predict too high lifetimes with more than a factor of 2. Calculated results with the presented model PJ-RifoT2 show a very good agreement with the experimental results under variable amplitude loading, especially under consideration of an improvement by the delay constant. In contrast to the results achieved with the original  $P_J$ -concept, the scattering of the ratio of calculated to experimental number of cycles to failure can be reduced from at least  $1/T_{10\%/90\%} = 2.98$  to  $1/T_{10\%/90\%} = 2.04$ . To evaluate the quality of the achieved results, the scattering of the results under variable amplitudes are compared to the scatter of experimental results under constant amplitude loading (see Figure 12). The shown scatter in the direction of fatigue life  $T_N$  is based on the calculated scatter in the direction of loading  $T_N$ . Shifting the derived Wöhler curve according to scattering in load direction leads to the shown scattering in direction of fatigue life, which increases with higher number of cycles in the range of HCF and the transition to endurance limit.

Within the scatter bands of 90%–10% and 95%–5%—in each case derived from constant amplitude loading

tests—lie 86% and 92% of the results under variable amplitude loading. This leads to the conclusion that the quality of the prediction under variable amplitude loading is in the order as the scattering of experimental results under constant amplitude loading. There is no option for further improvements unless enabling the prediction of scatter itself, for example, taking the influence of randomly arranged microstructure explicitly into account.

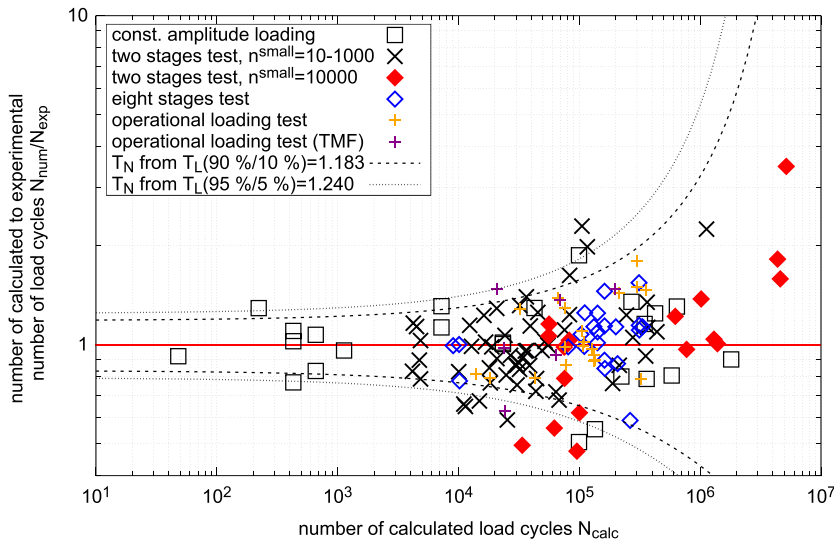
## 6 | DISCUSSION

### 6.1 | General

Based on the local concept generally and on the original  $P_J$ -concept more particularly, further variants were developed for damage assessment based on short crack growth. One of those developed variants has been presented in this paper: PJ-RifoT2. In contrast to the original  $P_J$ -concept, the modifications, extensions, and improvements can be summarized:

- Transformation from a damage accumulation to a crack growth calculation,
- Substitution of the crack growth law,





**FIGURE 12** Comparison of scattering of results under variable amplitude loading to scatter of results under constant amplitude loading [Colour figure can be viewed at [wileyonlinelibrary.com](http://wileyonlinelibrary.com)]

- Transformation of short crack threshold behavior on crack growth itself,
- Optimization of parameter identification,
- Modification of crack opening strains delay behavior,
- Consideration of transient crack closure,
- Consideration of temperature dependency.

## 6.2 | Transformation from a damage accumulation to a crack growth calculation

In the  $P_j$ -concept, the damage sum of the second run of the load spectrum was extrapolated to all possible further runs. The crack growth calculation resigns these simplifications. Therefore, even load cycles influence to crack opening strain, which damage first time after two runs through the load spectrum. This improvement, by running repeatedly through the load spectrum until the failure criterion ( $a = a_{end}$ ) is reached, ensures that the calculated fatigue lives are independent whether the load spectrum is defined as a multiple of an original load spectrum or not. Furthermore, it is possible to identify the exact load cycle which leads to the failure. When the load spectrum is applicable only a few times, the resulting difference in calculated runs through the load spectrum can be significant.

## 6.3 | Substitution of the crack growth law

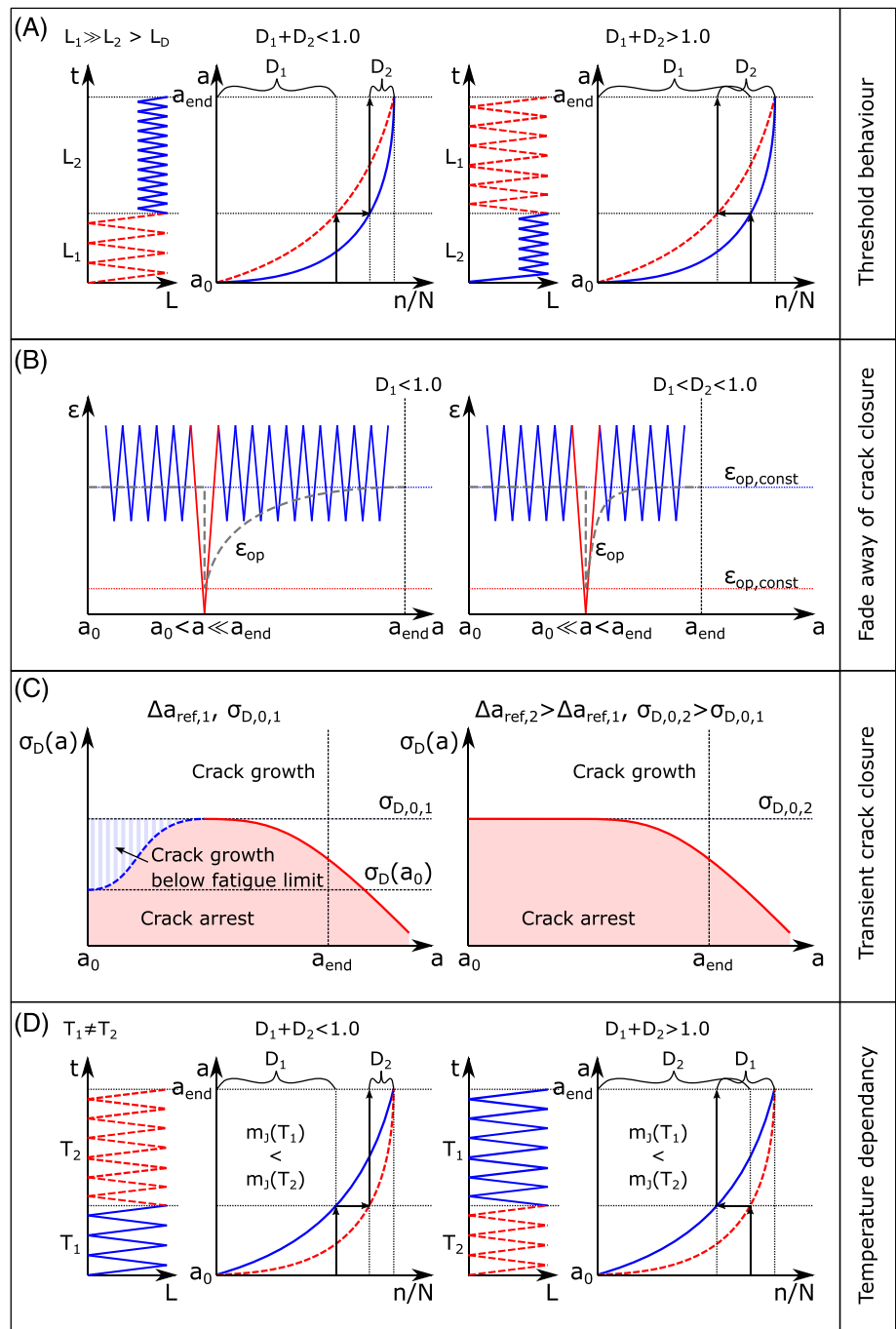
By replacing Equation (2) by Equation (3), the discontinuity in crack growth rate at the threshold is avoided. As

a consequence, derived life curve smoothly approaches the fatigue limit without a kink. However, a unique relation between crack length and the damage sum  $\sum n_i/N_i$  does no longer exist (Equation 5). Instead, it is from now on depending on the load level. Consequently, a new load sequence effect is accounted for in the calculation. For example, this means under a multiple step loading that a higher damage sum  $D = \sum n_i/N_i$  can be achieved when smaller cycles are applied at first instead of higher cycles. In reverse order of load application, the expected damage sum will be lower (see Figure 13a).

## 6.4 | Transformation of short cracks threshold behavior on crack growth itself

The transformation of short crack threshold behavior on crack growth itself is necessary due to the consideration of the threshold value in the crack growth law. A consideration of the microstructural length  $l^*$  on the load side (increased stress intensity at crack tip by fictive extension of the crack length) and not on the resistance side (reduced threshold value) offers several advantages. On the one hand, the identification of the parameters is much easier caused by a constant threshold value which effects that all essential parameters can mainly be identified analytically. On the other hand, it is possible to start crack growth calculations with an initial crack length of  $a_0 = 0$ . If, however, the crack growth constant  $C_j$  is predefined or the initial crack length is freely chosen, even under variable amplitude loading, there is no change in calculated fatigue life.

**FIGURE 13** Illustration of main additional load sequence effects by the developed concept [Colour figure can be viewed at wileyonlinelibrary.com]



### 6.5 | Modified delay behavior of crack opening strains

With the modified delay behavior of crack opening strains, the behavior was coupled to the crack length increments. Contrary to coupling to damage sum contributions, the delay behavior is slower for shorter cracks than for longer ones. This leads to a further load sequence effect. For the example of a single overload, the influence of the crack length-dependent delay behavior can be explained (see Figure 13b). For long

cracks and fast crack growth, the small cycles are less damaging because the state of stabilized crack closure is approached faster than for short cracks and slow crack growth.

### 6.6 | Transient crack closure behavior

The developed equation for transient crack closure behavior (crack length-dependent crack closure strain under constant amplitude loading) distinguishes from

Anthes<sup>15</sup> formulation. The crack length  $a$  is replaced by the increase of the crack length ( $a - a_0$ ). With this difference, cracks are fully open even for initial crack lengths  $a_0 > 0$ . In contrast to Anthes calculated delay constants (which was also adopted to FITNET Fitness-for-Service [FFS] Procedure<sup>66</sup>), the determined delay constants within the presented procedure are much smaller. This leads even to a much faster changes in the crack closure level. With the developed modification of the delay constant, the scattering in prediction accuracy was reduced by about 50% for this kind of tests.<sup>17</sup> For certain combinations of the delay constants  $\Delta a_{\text{ref}}$  and closure levels, crack arrest can be modeled for amplitudes at the fatigue limit and below. However, cracks grow at amplitudes below the initial fatigue limit, even under pulsating compression. For the case of crack arrest, the microstructural crack length  $l^*$  needs to be determined iteratively. Consequently, the dependent parameters have to be recalculated. Crack arrest induced by transient crack closure behavior is responsible for a further load sequence effect. The fatigue limit is to be understood as a state of crack arrest (see Murakami<sup>67</sup>). A schematic definition of a variable fatigue limit, based on the transient crack closure, is shown in Figure 13c.

## 6.7 | Temperature dependency

Consideration of temperature dependency was done by providing strain Wöhler curves in the temperature range of interest. This avoids inconsistencies in contrast to the damage parameter  $D_{\text{TMF}}$ <sup>33,35</sup> which considers the load side (by temperature-dependent material parameters) independently from the resistance side (by scaling the crack growth constant or alternatively the damage parameter). Neither calculated fatigue lives nor the fatigue limit can be described over large temperature ranges adequate to experimental findings under constant amplitude loading.<sup>17</sup> The deviations vary depending on the chosen reference temperature and the temperature-dependent material parameters itself. Motivated by these facts, a procedure was developed to determine the crack growth constants depending on temperature-dependent material parameters and the temperature-dependent damaging behavior under constant amplitude loading. Especially by modifying the crack growth exponent  $m_f(T)$ , additional load sequence effects result. In its consequence, the relation of the damage sum ( $n/N$ ) and crack length varies with the temperature. Here again, the result is a nonlinear damage accumulation (see Figure 13d).

## 6.8 | Comparison to FKM guideline nonlinear

The presented concept and the original  $P_J$ -concept and its applicable version published in the FKM guideline nonlinear<sup>11</sup> require as input the evaluated local stress strain paths by a hysteresis cycle count algorithm. The main difference between the presented concept and the FKM guideline nonlinear is here; local stress strain paths are calculated with the fatigue notch factor  $K_f$  (including notch supporting effects) instead of the stress concentration factor  $K_t$ . Calculated local stresses and strains are smaller, here. Therefore, load sequence effects originating from cyclic plasticity are here smaller, too. In the short crack growth regime, such sequence effects tend to reduce fatigue life. Smaller sequence effects result in longer calculated lives.

## 6.9 | Summarizing load sequence effects

Load sequence effects are considered by the local strain approach and the original  $P_J$ -concept due to:

- mean stress rearrangement by different load ratios from nominal to local,
- plasticity-induced crack closure,
- descending fatigue limit.

Additional load sequence effects introduced here are due to:

- substitution of crack growth equation with transformation of short cracks threshold behavior on crack growth itself,
- crack length-dependent delay of crack closure strain,
- transient crack closure behavior,
- temperature dependency.

Whether or not an effect is more important than another one depends on the load level, material behavior, and many other influencing parameters. Furthermore, the individual effects interact and influence each other.

## 6.10 | Application for other materials and possible extensions of the model

The extensive experimental investigations of various specimen geometries and load sequences form are a well-suited data basis for validating any life prediction concept. It was shown that the cyclic deformation

behavior under constant amplitude loading of the steel X6CrNiNb18-10 is characterized by a significant non-Masing behavior; further effects of cyclic hardening and softening are observable. Under strain-controlled variable amplitude loadings with load ratios different from  $-1$ , an additional mean stress relaxation is observed. Taking this mean stress relaxation into account for damage calculation leads to an improved quality of lifetime prediction. Another aspect, which has not been considered in damage calculation, is the cyclic hardening and softening due to plastic deformation; the calculations were done with idealized and stabilized cyclic material parameters neglecting non-Masing behavior. A so far neglected effect of cyclic hardening is an increase of the fatigue limit due to smaller plastic deformations.

No additional input parameters for the developed concept are needed in contrast to the original  $P_J$ -concept, which is one big advantage. For constant temperature, just a strain life curve, cyclic Ramberg–Osgood parameters, Young's modulus, and ultimate tensile strength are needed. Under variable temperature, these parameters need to be described temperature dependent.

The notch effect was just processed as a problem of transferability between unnotched and notched specimens. Whether an explicit consideration of the stress gradient, for example, done by Dankert<sup>68</sup>, may lead to additional improvements in the quality of lifetime prediction awaits investigation. Especially in combination with transient crack closure, it could result in a new dynamic of the crack arrest, with the consequences of a new assessment of the fatigue limit of notched bodies in contrast to unnotched bodies. In this context, it will also be required to review the applied method of the statistical support effect.

For thermomechanical loading, a reference temperature must be defined, and the equation for the effective cyclic  $J$ -integral has to be replaced, for example, according to Bauerbach, Schlitzer, and coauthors.<sup>56,69,70</sup>

Future developments should focus on the modeling of the transient cyclic deformation behavior. Such a modeling must be fast and efficient, against the background of several millions of cycles. Therefore, extensive FE calculations are excluded explicitly. During the investigations, only the mean stress relaxation in the nominal section of the notched specimens was considered for damage calculations. Locally in the notch, the effect of mean stress relaxation differs from behavior in the nominal section and is additionally combined with ratcheting, for example, shown by Panic.<sup>71</sup> The consideration of an additional mean stress relaxation combined with ratcheting in the notch is expected to provide improved fatigue assessment results.

## 7 | CONCLUSION

The presented model is an improvement and extension of the original  $P_J$ -model. The substitution of damage accumulation by crack propagation leads to new possibilities in the extension of the original model. Additional load sequence effects are accounted for by the transient and crack length-dependent crack closure formulation, the improved threshold behavior, and even the temperature-dependent crack growth exponent. These additional sequence effects resulted in the scatter of ratios of calculated and experimentally determined lifetimes under variable amplitude being comparable to the scatter under constant amplitude loading. Other materials should be considered for further validation.

## ACKNOWLEDGMENTS

Experimental findings were achieved within the IGF-project 18.842N “Erweiterte Schädigungskonzepte für thermomechanische Beanspruchung unter variablen Amplituden und plastischer Deformation” of the research association “Schweißen und verwandte Verfahren e.V.” of the DVS, Aachener Str. 172, 40223 Düsseldorf and funded by the AiF within the scope of the program for advancement of the industrial alliance of research (IGF) of the Federal Ministry for Economic Affairs and Energy on the basis of a decision by the German Bundestag. The financial support is greatly acknowledged. The research project was done together with Sophie Schackert and Christoph Schweizer from Fraunhofer Institute for Mechanics of Materials IWM, Freiburg, Germany. A majority of experimental results were achieved in Freiburg. We would like to thank them for the good and productive collaboration.

Open Access funding enabled and organized by Projekt DEAL.

## DATA AVAILABILITY STATEMENT


The data that support the findings of this study are available from the corresponding author upon reasonable request.

## NOMENCLATURE

$a_0^*$	estimated initial crack length including microstructural length $l^*$
$A_0, A_1, A_2, A_3$	coefficients for stabilized crack opening stress according to Newman
$C_J$	crack growth constant
$K_f$	effective stress concentration factor
$K_t$	stress concentration factor
$P_{50\%}$	mean value, 50% probability
$P_B$	damage parameter by Bergmann
$P_{J,D}$	calculated endurance limit in $P_J$ at initial crack length $a_0$ (PJ-Orig)

$P_{J,D}^{a=a_0}$	calculated endurance limit in $P_J$ at initial crack length $a_0$ (PJ-RifoT2)	$\Delta\epsilon_D$	double amplitude of endurance limit in strain $\epsilon_D$
$P_J$	damage parameter based on effective cyclic $J$ -integral	$\Delta\epsilon_{\text{eff}}$	effective strain range
$P_{\text{SWT}}$	damage parameter by Smith, Watson, and Topper	$\Delta\sigma_D$	double amplitude of endurance limit in stress $\sigma_D$
$R_\epsilon$	strain-controlled load ratio	$\Delta\sigma_{\text{eff}}$	effective stress range
$R_\sigma$	stress-controlled load ratio	$\Delta a$	crack length increment
$T_{10\% / 90\%}$	scattering by value ratio of 10%–90% probability	$D$	damage sum defined by $n/N$
$T_{\text{ref}}$	reference temperature	$E$	Young's modulus
$a_0$	initial crack length	$K'$	cyclic Ramberg–Osgood coefficient
$a_{\text{end}}$	crack length defined as failure	$N$	number of cycles to failure
$a_{\text{new}}$	new crack length after calculated cycle	$Q$	coefficient for $P_J$ -life curve
$l^*$	microstructural length	$T$	temperature
$m_J$	crack growth exponent	$a$	crack length
$n'$	cyclic Ramberg–Osgood exponent	$b, c$	exponents for strain Wöhler curve by Manson, Coffin, and Basquin
$\epsilon_{a,\text{max}}^{\text{higher}}$	maximum strain amplitude in load spectrum	$d$	diameter
$\epsilon_{a,\text{max}}^{\text{lower}}$	maximum strain amplitude of higher load spectrum	$n$	number of cycles
	maximum strain amplitude of lower load spectrum	$\Delta J_{\text{eff,th}}$	threshold for effective cyclic $J$ -integral
$\epsilon_{\text{cl,const}}$	stabilized strain at time of crack closure under const. amplitude loading	$\Delta J_{\text{eff}}$	effective cyclic $J$ -integral
$\epsilon_{\text{cl,const}}^a$	crack length-dependent strain at time of crack closure under const. amplitude loading	$\epsilon$	strain
$\epsilon_{\text{cl}}$	strain at time of crack closure	$\sigma$	stress
$\epsilon_D$	amplitude of endurance limit in strain under $R_\sigma = -1$ defined as $2 \cdot 10^6$ cycles		
$\epsilon_{\text{max,old}}$	drag pointer for upper reversal point in strain		
$\epsilon_{\text{max}}$	upper reversal point in strain		
$\epsilon_{\text{min,old}}$	drag pointer for lower reversal point in strain		
$\epsilon_{\text{min}}$	lower reversal point in strain		
$\epsilon_{\text{op,const}}$	stabilized strain at time of crack opening under const. amplitude loading		
$\epsilon_{\text{op,const}}^a$	crack length-dependent strain at time of crack closure under const. amplitude loading		
$\epsilon_{\text{op,new}}$	strain at time of crack opening left by the actual cycle		
$\epsilon_{\text{op,prev}}$	left strain at time of crack opening of the previous cycle		
$\epsilon_{\text{op}}$	strain at time of crack opening		
$\sigma_0$	simplified yield stress		
$\sigma_a$	stress amplitude		
$\sigma_{\text{cl}}$	stress at time of crack closure		
$\sigma_D$	amplitude of endurance limit in stress under $R_\sigma = -1$ defined as $2 \cdot 10^6$ cycles		
$\sigma_{\text{max}}$	upper reversal point in stress		
$\sigma_{\text{min}}$	lower reversal point in stress		
$\sigma_{\text{op}}$	stress at time of crack opening		
$\sigma'_f, \epsilon'_f$	coefficients for strain Wöhler curve by Manson, Coffin, and Basquin		
$\Delta a_{\text{ref}}$	fadeaway constant for crack closure strain		

## ORCID

Alexander Bosch  <https://orcid.org/0000-0002-0954-443X>

Michael Vormwald  <https://orcid.org/0000-0002-4277-785X>

## REFERENCES

1. KTA 3201.2. Komponenten des Primärkreises von Leichtwasserreaktoren Teil 2: Auslegung, Konstruktion und Berechnung. 2013.
2. ASME boiler pressure vessel code section VIII division 2. Alternative rules, rules for construction of pressure vessels. 2007.
3. Palmgren A. Die Lebensdauer von Kugellagern. *VDI-Z.* 1924; 68(14):339-341.
4. Miner MA. Cumulative damage in fatigue. *Trans ASME J Appl Mech.* 1945;12(6):359-365.
5. Vormwald M. Classification of load sequence effects in metallic structures. *Procedia Eng.* 2015;101:534-542.
6. Fatemi A, Yang L. Cumulative fatigue damage and life prediction theories: a survey of the state of the art for homogeneous materials. *Int J Fatigue.* 1998;20(1):9-34.
7. Skorupa M. Load interaction effects during fatigue crack growth under variable amplitude loading - a literature review. Part I: empirical trends. *Fatigue Fract Eng Mater Struct.* 1998;21(8): 987-1006.
8. Skorupa M. Load interaction effects during fatigue crack growth under variable amplitude loading-a literature review. Part II: qualitative interpretation. *Fatigue Fract Eng Mater Struct.* 1999;22(10):905-926.
9. Dowling NE. 4.03 - Local strain approach to fatigue. In: Ritchie RO, ed. *Comprehensive Structural Integrity.* Oxford: Pergamon; 2003:77-94.

10. Fiedler M, Vormwald M. Considering fatigue load sequence effects by applying the local strain approach and a fracture mechanics based damage parameter. *Theor Appl Fract Mech*. 2016;83:31-41.
11. Fiedler M, Wächter M, Varfolomeev I, Vormwald M, Esderts A. *Richtlinie Nichtlinear: Rechnerischer Festigkeitsnachweis unter expliziter Erfassung nichtlinearen Werkstoffverformungsverhaltens für Bauteile aus Stahl, Stahlguss und Aluminiumknetlegierungen*. 1sted. Frankfurt am Main: VDMA Verlag GmbH; 2019.
12. Vormwald M, Seeger T. The consequences of short crack closure on fatigue crack growth under variable amplitude loading. *Fatigue Fract Eng Mater Struct*. 1991;14(2/3):205-225.
13. Vormwald M, Heuler P, Seeger T. A fracture mechanics based model for cumulative damage assessment as part of fatigue life prediction. In: Mitchell MR, Landgraf RW, eds. *Advances in Fatigue Life Prediction Techniques*. Philadelphia: ATSM; 1992: 28-46.
14. Vormwald M, Heuler P, Krä C. Spectrum fatigue life assessment of notched specimens using a fracture mechanics based approach. In: Amzallag H, ed. *Automation in Fatigue and Fracture: Testing and Analysis*. West Conshohocken, PA: ASTM; 1994:219-231.
15. Anthes RJ. Ein neuartiges Kurzzriffschrittsmodell zur Anrißlebensdauervorhersage bei wiederholter Beanspruchung. Report 57: Inst. f. Stahlbau und Werkstoffmechanik, TU Darmstadt. 1997.
16. Bosch A, Vormwald M. Concepts for crack propagation under variable mechanical and thermal loadings based on the effective cyclic J-integral. In: Decker M, ed. *VAL4 - Fourth International Conference on Material and Component Performance under Variable Amplitude Loading*. Berlin: DVM; 2020:323-332.
17. Schackert S, Bosch A, Schweizer C, Vormwald M. Erweiterte Schädigungskonzepte für thermomechanische Beanspruchung unter variablen Amplituden und plastischer Deformation. Report AiF-No. 18.842. 2018.
18. Schackert S, Schweizer C, Vormwald M, Bosch A. Lebensdauerbewertung geschweißter Rohrleitungen aus dem austenitischen Stahl 1.4550 mithilfe von Kurzzrisswachstumsmodellen. *Schweißen Und Schneiden*. 2019; 5:286-292.
19. Bosch A. Kurzzrisswachstumsmodelle unter Berücksichtigung variabler strukturmechanischer und thermischer Belastung. Report 127: Inst. f. Stahlbau u. Werkstoffmechanik, TU Darmstadt. 2019.
20. Smaga B, Daniel S, Sorich B. Fatigue behavior of metastable austenitic stainless steels in LCF, HCF and VHCF regimes at ambient and elevated temperatures. *Metals*. 2019;9(6):704.
21. Bayerlein M, Christ H-J, Mughrabi H. Plasticity-induced martensitic transformation during cyclic deformation of AISI 304L stainless steel. *Mater Sci Eng A*. 1989;114:L11-L16.
22. Dynamic Systems. Gleeble 540: welding simulator. 2021; <https://www.bleeble.org/products/gleeble-systems/welding-simulator.html>.
23. Neuber HH. Theory of stress concentration for shear-strained prismatical bodies with arbitrary nonlinear stress-strain law. *J Appl Mech*. 1961;24(4):544-550.
24. Rennert R, Kullig E, Vormwald M, Esderts A, Siegele D. *Rechnerischer Festigkeitsnachweis für Maschinenbauteile aus Stahl, Eisenguss- und Aluminiumwerkstoffen*. 6thed. Frankfurt am Main: VDMA-Verl; 2012.
25. Bosch A, Schackert S, Schweizer C, Vormwald M. Fatigue life assessment of welded joints made of the stainless steel X6CrNiNb18-10 for thermomechanical and variable amplitude loading. *Mater Sci Eng Technol*. 2018;49(3):316-331.
26. Ramberg W, Osgood W. Description of stress-strain curves by three parameters. 1943.
27. Finney DJ. *Probit Analysis*. London: Cambridge University Press; 1947.
28. Lemaitre J, Chaboche J-L. *Mechanics of Solid Materials*. Cambridge: Cambridge University Press; 1990.
29. Döring R. Zum Deformations- und Schädigungsverhalten metallischer Werkstoffe unter mehrachsig nichtproportionalen zyklischen Beanspruchungen. Report 57: Inst. f. Stahlbau und Werkstoffmechanik, TU Darmstadt. 2006.
30. Fang J. *Cyclic Plasticity Modelling and Multiaxial Fatigue Assessment for an Austenitic Steel*. München: Herbert Utz Verlag GmbH; 2015.
31. Bosch A, Vormwald M. Rissfortschrittskonzepte auf Grundlage des effektiven zyklischen J-Integrals für Strukturen unter variabler strukturmechanischer und thermischer Belastung. In: 51. Tagung des Arbeitskreises Bruchmechanik und Bauteilsicherheit. 2019, pp. 137-148.
32. Bosch A, Schackert S, Schweizer C, Vormwald M. Fatigue life of welded joints of AISI 347 stainless steel under thermomechanical and variable amplitude loading. In: Proc. of the ASME Pressure Vessels and Piping Conference. 2018.
33. Riedel H. *Fracture at High Temperatures*. Berlin, Heidelberg, New York: Springer-Verlag; 1987.
34. Maier G, Möser M, Riedel H, Seifert T, Siegele D, Klöwer J et al. High temperature plasticity and damage mechanisms of the nickel alloy 617B. In: Proc. of the 36th MPA-Seminar Materials and Components Behaviour in Energy & Plant Technology. 2010.
35. Schmitt W, Mohrmann R, Riedel H, Dietsche A, Fischersworing-Bunk A. Modelling of the fatigue life of automobile exhaust components. In: Proc. of the 8th International Fatigue Congress. 2002;781-788.
36. Seifert T, Schweizer C, Schlesinger M, Möser M, Eibl M. Thermomechanical fatigue of 1.4849 cast steel – experiments and life prediction using a fracture mechanics approach. *IJMR (Int J Mater Res)*. 2010;101(8):942-950.
37. Schweizer C, Seifert T, Nieweg B, von Hartrott P, Riedel H. Mechanisms and modelling of fatigue crack growth under combined low and high cycle fatigue loading. *Int J Fatigue*. 2011;33(2):194-202.
38. Heitmann HH, Vehoff H, Neumann P. Random load fatigue of steels: service life prediction based on the behaviour of microcracks. In: Proc of the Int Conf. Appl. of Fract. Mech. to Mat. and Struct., 1993
39. Heitmann HH. Betriebsfestigkeit von Stahl: Vorhersage der technischen Anrißlebensdauer unter Berücksichtigung des Verhaltens von Mikrorissen: Fak. für Bergbau und Hüttenwesen, RWTH Aachen. 1983.
40. Kamaya M, Kawakubo M. Loading sequence effect on fatigue life of type 316 stainless steel. *Int J Fatigue*. 2015;81:10-20.
41. Liang W, Conle FA, Topper TH, Walbridge S. A review of effective-strain based and multi R-ratio crack propagation

- models and a comparison of simulated results using the two approaches. *Int J Fatigue*. 2021;142:105920.
42. Vormwald M. Anrißlebensdauervorhersage auf der Basis der Schwingbruchmechanik für kurze Risse. Report 47: Inst. f. Stahlbau und Werkstoffmechanik, TH Darmstadt. 1989.
  43. Dowling NE. J-integral estimates for cracks in infinite bodies. *Eng Frac Mech*. 1987;26(3):333-348.
  44. El Haddad MH, Dowling NE, Topper TH, Smith KN. J integral applications for short fatigue cracks at notches. *Int J Fract*. 1980;16(1):42-46.
  45. Tanaka K, Nakai Y, Yamashita M. Fatigue growth threshold of small cracks. *Int J Fatigue*. 1981;17(5):519-533.
  46. Newman JC Jr. A crack opening stress equation for fatigue crack growth. *Int J Fract*. 1984;24(4):R131-R135.
  47. Chopra OK, Shack WJ. Effect of LWR coolant environments on the fatigue life of reactor materials. U.S. Nuclear Regulatory Commission, Office of Nuclear Regulatory Research, Washington, DC. 2007.
  48. Ebi G G, Riedel H, Neumann P. Fatigue life prediction based on microcrack growth. In: Proc. 6th European Conf. Fracture 1986;1587-1598.
  49. Gavenda DJ, Luebbers PR, Chopra OK. Crack initiation and crack growth behavior of carbon and low-alloy steels. 1997.
  50. Suresh S, Ritchie R. Propagation of short fatigue cracks. *Int Met Rev*. 1984;29:445-476.
  51. Dowling NE, Begley JA. Fatigue crack growth during gross plasticity and the J - integral. In: Rice J, Paris P, eds. *Mechanics of Crack Growth*. West Conshohocken, PA: ASTM; 1976:82-103.
  52. Gamache B, McEvily AJ. On the development of fatigue crack closure. In: Bailon J-P, Dickson JI, eds. *Fatigue 93. Proc. 5th Int. Conf. on Fatigue and Fatigue Thresholds*. Warley, UK: EMAS; 1993:577-582.
  53. Heuler P. Anrißlebensdauervorhersage bei zufallsartiger Belastung auf der Grundlage örtlicher Beanspruchungen. Report 40: Inst. f. Stahlbau und Werkstoffmechanik, TH Darmstadt. 1983.
  54. Taylor D. *A Compendium of Fatigue Thresholds and Growth Rates*. Warley: Engineering Materials Advisory Services; 1985.
  55. Southwest Research Institute. NASGRO v6.1 Release Notes. 2010.
  56. Bauerbach K, Beier HT, Fischaleck M, Rudolph J, Schlitzer T, Scholz A et al. Numerische Simulation und experimentelle Charakterisierung des Ermüdungsrischwachstums unter thermozyklischer Beanspruchung. Report BMBF 02NUK009D H 139457. Darmstadt. 2013.
  57. Schuler X, Herter K-H, Rudolph J. Derivation of design fatigue curves for austenitic stainless steel grades 1.4541 and 1.4550 within the German Nuclear Safety Standard KTA 3201.2. In: Proc. of the ASME Pressure Vessel and Piping Conference. 2013.
  58. Langer BF. Design of pressure vessels for low-cycle fatigue. *J Basic Eng*. 1962;84(3):389-399.
  59. Manson SS. Behaviour of materials under conditions of thermal stress. NACA: TN-2993. 1953.
  60. Coffin LF Jr. A study of the effects of cyclic thermal stresses on a ductile metal. *Trans ASME*. 1954;76:931-950.
  61. Basquin OH. The exponential law of endurance tests. *Am Soc Test Mater*. 1910;10:625-630.
  62. Morrow JD. Cyclic plastic strain energy and fatigue of metals. In: Lazan B, ed. *Internal Friction, Damping, and Cyclic Plasticity*. West Conshohocken, PA: ASTM; 1965:45-87.
  63. Smith KN, Watson P, Topper TH. A stress-strain function for the fatigue of metals. *J Mater*. 1970;5(4):767-778.
  64. Bergmann JW. Zur Betriebsfestigkeitsbemessung gekerbter Bauteile auf der Grundlage der örtlichen Beanspruchungen. Report 37: Inst. f. Stahlbau und Werkstoffmechanik, TH Darmstadt. 1983.
  65. Rossow E. Eine einfache Rechenschiebernäherung an die den normal scores entsprechenden Prozentpunkte. *Qualitätskontrolle*. 1964;9(12):146-147.
  66. Koçak M, Webster S, Janosch JJ, Ainsworth RA, Koers R. *FIT-NET Fitness-for-Service (FFS) - Procedure*. Vol. 1. 1sted. GKSS Geesthacht; 2008.
  67. Murakami Y. *Metal Fatigue: Effects of Small Defects and Non-metallic Inclusions*. USA: Elsevier; 2002.
  68. Dankert M. Ermüdungsrischwachstum in Kerben - Ein einheitliches Konzept zu Berechnung von Anriß- und Rißfortschrittslebensdauern. Report 60: Inst. f. Stahlbau und Werkstoffmechanik, TU Darmstadt. 1999.
  69. Schlitzer T, Bauerbach K, Beier HT, et al. Experimental characterization and numerical assessment of fatigue crack growth under thermo-mechanical conditions. *Mat -Wiss U Werkstofftech*. 2015;46(2):165-177.
  70. Bauerbach K. Numerische Betrachtungen zu Deformationsverhalten und Schädigungsbewertung kurzer Risse unter thermozyklischer Beanspruchung. Report 103: Inst. f. Stahlbau und Werkstoffmechanik, TU Darmstadt. 2014.
  71. Panic D, Beier TH, Vormwald M. Damage assessment of threaded connections based on an advanced material model and local concepts. *Procedia Eng*. 2014;74:119-128.

**How to cite this article:** Bosch A, Vormwald M. Modeling short crack propagation under variable structural and thermal loadings. *Fatigue Fract Eng Mater Struct*. 2021;44:1652-1674. <https://doi.org/10.1111/ffe.13447>